Article

Cell Host & Microbe

On-person adaptive evolution of *Staphylococcus aureus* during treatment for atopic dermatitis

Graphical abstract

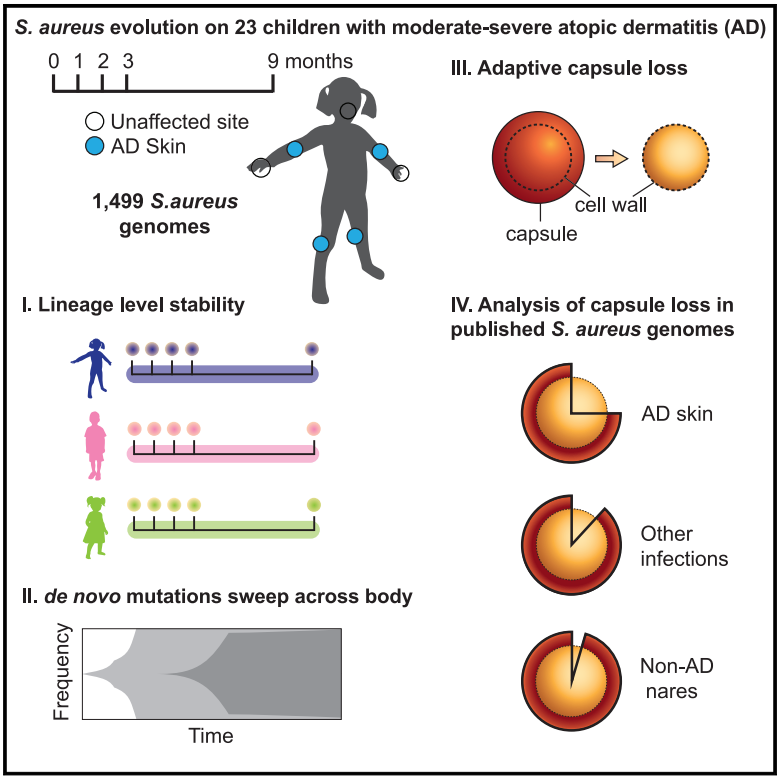

Highlights

- Most patients are colonized stably by a single *S. aureus* sequence type
- Within each lineage, *de novo* variants spread and replace their on-person ancestors
- On-person and across-person parallel evolution is observed in *capD*
- Capsule loss enriched on AD patients compared with healthy carriage or other diseases

Authors

Felix M. Key, Veda D. Khadka, Carolina Romo-González, ..., Isaac M. Chiu, Maria T. García-Romero, Tami D. Lieberman

Correspondence

mgarciar@pediatria.gob.mx (M.T.G.-R.), tami@mit.edu (T.D.L.)

In brief

Key et al. investigate the spatial and temporal evolution of *S. aureus* on children with atopic dermatitis (AD). Patients are stably colonized by a single lineage; however, mutations emerge within each lineage and spread across the body. Mutations in a capsule production gene showed signatures of context-dependent adaptation.

Key et al., 2023, Cell Host & Microbe *31*, 593–603
April 12, 2023
https://doi.org/10.1016/j.chom.2023.03.009

CellPress

Cell Host & Microbe

CellPress
OPEN ACCESS

Article

On-person adaptive evolution of *Staphylococcus aureus* during treatment for atopic dermatitis

Felix M. Key,[1,2,9] Veda D. Khadka,[1,2] Carolina Romo-González,[3] Kimbria J. Blake,[4,10] Liwen Deng,[4] Tucker C. Lynn,[1,2] Jean C. Lee,[5] Isaac M. Chiu,[4] Maria T. García-Romero,[6,*] and Tami D. Lieberman[1,2,7,8,11,*]

[1]Institute for Medical Engineering and Science, Massachusetts Institute of Technology, Cambridge, MA, USA
[2]Department of Civil and Environmental Engineering, Massachusetts Institute of Technology, Cambridge, MA, USA
[3]Experimental Bacteriology Laboratory, National Institute for Pediatrics, Mexico City, Mexico
[4]Department of Immunology, Blavatnik Institute, Harvard Medical School, Boston, MA, USA
[5]Division of Infectious Disease, Department of Medicine, Brigham and Women's Hospital and Harvard Medical School, Boston, MA, USA
[6]Department of Dermatology, National Institute for Pediatrics, Mexico City, Mexico
[7]Broad Institute, Massachusetts Institute of Technology, Cambridge, MA, USA
[8]Ragon Institute, Massachusetts Institute of Technology, Cambridge, MA, USA
[9]Present address: Max Planck Institute for Infection Biology, 10117 Berlin, Germany
[10]Present address: Genoskin Inc., Salem, MA, USA
[11]Lead contact
*Correspondence: mgarciar@pediatria.gob.mx (M.T.G.-R.), tami@mit.edu (T.D.L.)
https://doi.org/10.1016/j.chom.2023.03.009

SUMMARY

The opportunistic pathogen *Staphylococcus aureus* frequently colonizes the inflamed skin of people with atopic dermatitis (AD) and worsens disease severity by promoting skin damage. Here, we show, by longitudinally tracking 23 children treated for AD, that *S. aureus* adapts via *de novo* mutations during colonization. Each patient's *S. aureus* population is dominated by a single lineage, with infrequent invasion by distant lineages. Mutations emerge within each lineage at rates similar to those of *S. aureus* in other contexts. Some variants spread across the body within months, with signatures of adaptive evolution. Most strikingly, mutations in capsule synthesis gene *capD* underwent parallel evolution in one patient and across-body sweeps in two patients. We confirm that *capD* negativity is more common in AD than in other contexts, via reanalysis of *S. aureus* genomes from 276 people. Together, these findings highlight the importance of the mutation level when dissecting the role of microbes in complex disease.

INTRODUCTION

During the colonization of human microbiomes, bacteria acquire adaptive mutations that enhance their ability to survive in the human environment, resist antibiotics, and outcompete other strains.[1–4] Although these *de novo* mutations rise in frequency due to the survival advantage they provide to the bacteria, their emergence may impact host metabolism, immune homeostasis, or microbiome dynamics. Understanding the tempo and consequences of variations across bacterial genomes is of particular importance for complex inflammatory diseases such as atopic dermatitis (AD) and inflammatory bowel diseases, for which the causative role of the microbiome has been hard to pin down.[5,6] Although recent studies have identified bacterial strains associated with inflammatory states,[7–9] classic metagenomic approaches do not provide the resolution to robustly identify individual mutations emerging in disease states. As a result, the potential impact of *de novo* microbiome mutations on complex diseases is poorly understood.

AD is one such chronic inflammatory skin disease with strong microbial associations and a complex etiology. AD transiently affects up to 20% of people during their lifetime[10] and is particularly prominent among children, who develop itchy patches of inflamed skin, typically located on the cubital and popliteal fossae (inside of elbows and backs of knees).[11] Genetic and environmental defects in barrier function have been associated with AD but are insufficient to explain the variation in disease development and response to treatment.[12] Notably, symptomatic AD skin of children and adults is usually colonized by the opportunistic pathogen *Staphylococcus aureus*, with abundance proportional to disease severity[13–18]; this species is usually lowly abundant on healthy skin.[19,20] Its native reservoir is believed to be the nares, where it asymptomatically colonizes 30% of healthy individuals.[19] However, *S. aureus* also causes various human infections of the skin, bloodstream, lung, and bone.[21]

S. aureus sequence types vary in virulence potential, in the antibiotic resistance cassettes they carry, and the disease contexts in which they are most often found (e.g., hospital or community associated)[21,22]; however, no sequence types have been robustly associated with AD.[23] A recent study has suggested that *de novo* mutations in a key quorum sensing pathway

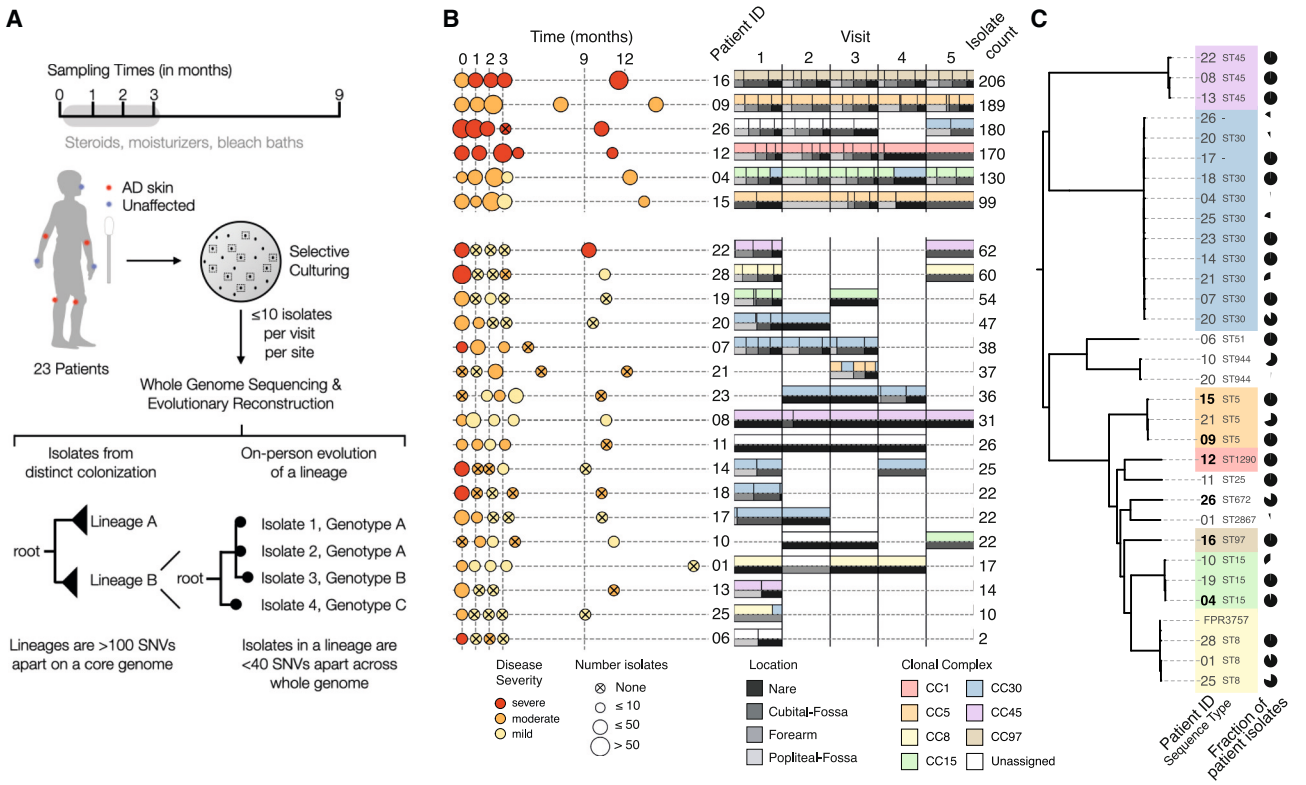

Figure 1. The *S. aureus* population on each child with atopic dermatitis (AD) is dominated by a single, stable, patient-specific lineage

(A) Swab samples were collected from each of 7 sites during each of 5 visits, including from nares and areas rarely affected by AD in children (forearms). Patient treatment for AD with standard treatment of care, with or without bleach baths, was monitored closely between the first four visits (STAR Methods). From each swab, up to 10 colonies were cultured and processed for whole-genome sequencing. We then grouped isolates from each patient into lineages such that isolates from the same lineage are fewer than 100 mutations across the core genome and performed more detailed evolutionary analysis using alignment of raw reads to lineage-specific assemblies built from reads of all isolates in a lineage. Isolates separated by 0 mutations in this more detailed analysis are then grouped into a single genotype.

(B) Left panel: sampling time, mean disease severity at visit based on SCORAD (mild < 25 ≤ moderate < 50 ≤ severe), and number of isolates per visit (dot size) are shown for each patient. Some sampling visits deviated from the anticipated schedule (vertical dashed line), spacing shown reflects the actual sampling schedule achieved (STAR Methods). Right panel: pairwise stacked bar plots show the relative number of isolates from each visit that were from an inferred clonal complex (top) and sampling site (bottom). Small vertical lines separate groups of isolates from the same site and clonal complex. Six patients with ≥99 isolates were analyzed with the most detail.

(C) Phylogenetic tree showing the relationship between 1,499 *S. aureus* isolates, generated using 60,973 SNVs from a reference-based approach (STAR Methods) and labeled by patient of origin and sequence type. Pie charts indicate the fraction of patient isolates that come from each lineage, showing most patients have a single major lineage. Patient 20 was colonized by three lineages, two of which are part of the same clonal complex (CC30). Lineages are colored according to their assigned clonal complex (STAR Methods), highlighting that strains colonizing AD patients come from a wide variety of global diversity.

reduce the risk for healthy babies to develop AD[24]—supporting a possible role for *S. aureus* mutations beyond the strain level in AD. Although *de novo* mutations occurring in *S. aureus* in young children with AD have been observed,[25] the fate of these mutations over time and their consequences have not been characterized.

RESULTS

Longitudinal tracking of *S. aureus* evolution in AD

Here, we use longitudinal sampling and culture-based whole-genome sequencing to identify mutations acquired by *S. aureus* that emerge under natural selection in individual people. We conducted a prospective, longitudinal study of 23 children (aged 5–15 years old) in Mexico with moderate to severe AD at 5 visits over the course of approximately 9 months (Figure 1A). Patients were treated for AD with the standard of care, including topical steroids, emollients, and some with bleach baths. Treatment was modified at each visit according to severity, although patients were not closely followed up between the fourth and the final visits (Table S1). Three of the 23 patients were administered antibiotics in this initial period due to medical need, and 5 took antibiotics after this initial period; these patients were included in the analysis, and antibiotic usage is noted (see Table S1 for details). During each visit, AD severity was assessed using the scoring AD (SCORAD) scale,[26] and swabs were collected from seven affected and unaffected skin sites, including cubital and popliteal fossae, forearms, and the nares (Figure 1A). From each of the 225 swabs that yielded growth resembling *S. aureus*, we picked up to 10 single-colony isolates for subculture and sequencing (STAR Methods), resulting in 1,499 *S. aureus* whole genomes.

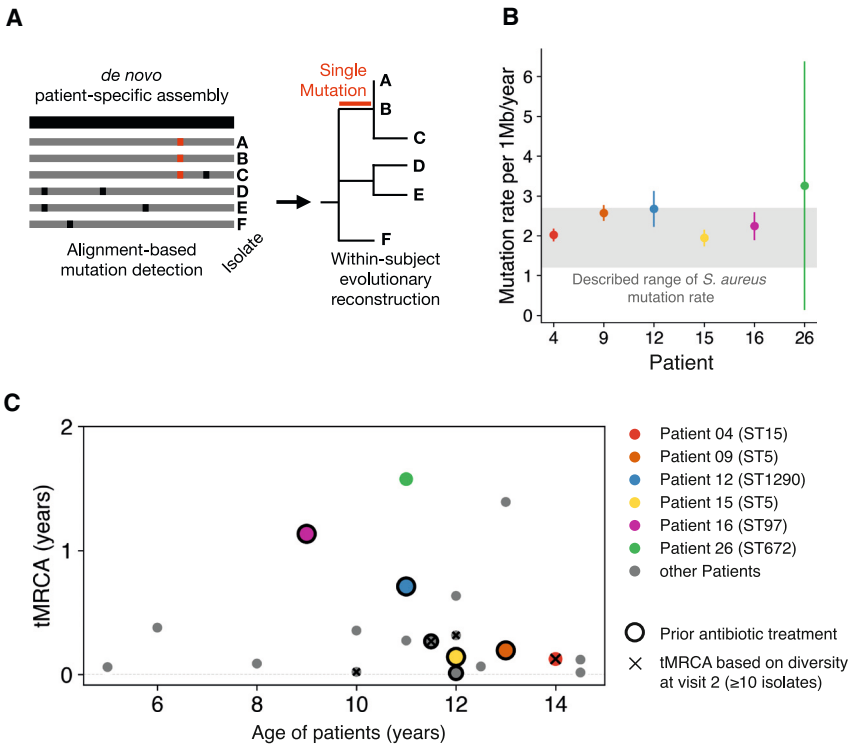

Figure 2. Despite high rates of mutation accumulation on each person, the intralineage diversity on each person is limited

(A) We built a *de novo* reference genome for each patient's major lineage (black) and called *de novo* mutations by aligning raw reads from each sample individually to the corresponding reference genome, allowing the building of fine-resolution phylogenetic trees (STAR Methods).

(B) The median molecular clock rate per megabase (Mb) is shown for the six patients with the most isolates (linear least-squares regression). Error bars indicate 95% confidence intervals. The gray region indicates per Mb clock rates reported for *S. aureus* in other contexts, corresponding to approximately 3–8 mutations per genome per year.[27–32]

(C) For each patient with ≥10 isolates at a visit (20 patients), the inferred time elapsed since the population's most recent common ancestor (tMRCA; STAR Methods) is plotted relative to the patient's age. Low values of tMRCA indicate a recent single-cell bottleneck and are found across patients, regardless of antibiotic usage within the past 6 months (black outline) or age. The earliest such visit from each patient was used; x's indicate patients for which visit 2 was used. Mutational distances were converted to time using the calculated molecular clocks for the 6 highlighted patients; for all others, the median rate was used.

To understand the minimal number of independent colonizations of *S. aureus* onto each child, we first clustered each patient's isolates into lineages, where each lineage is composed of isolates separated by <100 mutations across the core genome. Given the known rates of mutation accumulation in *S. aureus* in other contexts (~8 mutations/whole genome/year),[27–32] this cutoff ensures that all isolates that could have theoretically arisen from a single colonization and subsequent on-person diversification are grouped together. In practice, isolates from the same lineage are always less than 40 single-nucleotide variants (SNVs) apart across core and whole genomes and share the same multi-locus sequence type used in traditional *S. aureus* epidemiology (Figure S1; Table S1).

Most patients were stably colonized by a single major lineage, although we recovered minority lineages from 7 patients and major lineage replacements in 2 of the 19 patients with *S. aureus* recovered at multiple time points (Figure 1B; Table S2). Overall, detected lineages span the diversity of the *S. aureus* species (Figure 1C).[33] The largest fraction of lineages are part of clonal complex 30 (33% of lineages; 15% of isolates), in contrast with a previous finding of clonal complex 1 dominance among people with AD in the United Kingdom.[25]

The number of isolates recovered per visit from which sufficient sequencing reads were obtained is variable across visits and correlates with both disease severity and *S. aureus* relative abundance inferred from 16S rRNA sequencing[18] (0–68 isolates/visit; r^2 = 0.36 and r^2 = 0.16, respectively; Figures 1B and S2). Six patients provided large numbers of isolates amenable to more in-depth quantitative analyses (99–206 isolates/patient; Figure 1B).

S. aureus mutants sweep across the body

To analyze the causes and consequences of bacterial mutation on each person, we next focused on the genetic variation within each stably colonizing lineage. For each patient's major lineage, we generated a lineage-specific *S. aureus* assembly, used a rigorous alignment-based approach to identify SNVs, and built phylogenetic trees that illustrated mutation accumulation on the patient (Figure 2A; STAR Methods). In many cases, multiple colonies from a time point were indistinguishable across their entire genome; we refer to each group of isolates with identical genomes as a "genotype."

In theory, the inflammatory environment on AD skin, or the application of treatments to the skin, might induce an elevated mutation rate. We estimated the molecular clock of the lineages colonizing the six patients with the most isolates. For five of these patients' lineages, molecular clock estimates were consistent with those of *S. aureus* in other contexts, including healthy carriage and in invasive infections (1.2–2.7 × 10^{-6} substitutions/site/year[27–32]; Figure 2B). Patient 26's major lineage had an apparently higher accumulation mutation rate of 3.3 × 10^{-6} substitutions/site/year (CI95 = 0.1–6.4 × 10^{-6} substitutions/site/year), but this difference was not significant. Although this non-significantly elevated mutation accumulation rate could plausibly reflect environmental conditions that induced higher mutagenesis or a defect in DNA repair, we do not observe any mutations in DNA repair genes or significant differences in mutational spectra across patients (Figure S3). Taken as a whole, these results suggest that AD-associated inflammation does not greatly increase *S. aureus* mutation rates.

Accumulation of mutations over time can produce two different patterns of on-person evolution: diversification into long co-existing genotypes or within-lineage genotypic replacement.[34,35] To determine which of these patterns was more common, we calculated the time since each major lineage's isolates shared a single-celled ancestor (time to the most recent common ancestor [tMRCA]). We found that all 16 patients with sufficient data at the first visit ($\geq$10 isolates) had low values of tMRCA, indicating the seeding of the population from a single genotype within the past few years (tMRCA < 1.6 years; Figure 2C). We did not find a dependence on recent antibiotic usage ($p = 0.81$; two-sided Wilcoxon rank-sum test). In addition, similarly low values of tMRCA were found for samples collected after the initiation of study-related treatment (major lineages where visit 1 yielded $\leq$10 isolates; Figure 2C) and in a reanalysis of 8 AD patients from an unrelated study from which $\geq$10 isolates were collected at a single time point (Figure S4). Together with our observations of lineage-level stability (Figure 1B), these analyses suggest that within-lineage genotypic replacement is a common aspect of *S. aureus* growing on treated AD skin.

To better understand within-lineage replacement, we examined within-patient phylogenies for all patients (Figures 3, S5, and S6). Visualizing the temporal evolutionary dynamics using Muller diagrams revealed a common pattern in which genotypes with newly acquired mutations repeatedly replaced the existing diversity (Figures 3A–3F). These replacements spanned the entire body; the spread of new mutations was not spatially restricted and included unaffected skin and the natural habitat of the nose (Figures 3G, 3H, S5, and S6). For time points from which *S. aureus* was cultured from more than one site, new mutations are typically found at multiple body sites—making it difficult to tell at which site they originated. Although some of these sweeps overlapped with antibiotic administration between samplings, many intervals without antibiotic usage demonstrate similarly dramatic changes in mutational composition, further supporting the presence of an antibiotic-independent mechanism of genotypic sweeps.

The ladder-like phylogenies we observe here, showing a succession of closely related genotypes, strongly support a role for on-person mutation, rather than transmission from another person or outside source (e.g., Figure 3H). In theory, however, these phylogenies could arise if transmission between individuals was so frequent that there were back-and-forth transmissions between each pair of visits. To understand the intraperson transfer, we examined one pair of siblings in our dataset. These siblings share closely related lineages separated by 14 mutations, corresponding to a MRCA about 17.4 months before the start of the study (95% confidence interval: 16.2–19 months). Despite this evidence of a recent shared ancestor, the siblings' populations do not share mutations derived during the study period—further supporting the notion that on-person evolution drives on-person phylogenetic diversity (Figure S1F). Altogether, these analyses suggest that new *S. aureus* genotypes commonly emerge via on-person *de novo* mutation in people being treated for AD, some of which subsequently sweep the on-person population.

Adaptive mutations alter polysaccharide capsule

The speed of genotype replacement raises the possibility that the underlying mutations provide a competitive advantage on AD skin. To test whether this process was adaptive, or arose from a neutral bottleneck (e.g., a reduction in cell number during treatment and subsequent growth), we investigated mutated genes for adaptive signatures. We first searched for evidence of parallel evolution, i.e., multiple mutations in the same gene within a single patient.[34] In patient 12, we observed four different mutations in *capD*, each in separate isolates. This mutational density is unlikely, given the small number of mutations in this patient ($p = 1.7 \times 10^{-5}$, simulation), and all four mutations resulted in either amino acid replacement or a premature stop codon, further supporting an adaptive role for mutations in this gene (Figure 3G). The *capD* gene encodes an enzyme that performs the first step in synthesizing the capsular polysaccharide of *S. aureus*. One of the *capD* mutations in patient 12, premature stop codon E199*, is associated with a spread and replacement event in this patient (1 of 11 mutations associated with replacement in this patient). Strikingly, a spread and replacement event in patient 9 is also associated with a mutation in *capD*: a nonsynonymous N595S mutation (Figure 3H). Although isolates containing the N595S mutation have detectable capsule expressions (STAR Methods; Table S3), this amino acid position is conserved within *S. aureus* and may be critical for native capsule structure (Figure S7). These observations of parallel evolution within a patient, parallel evolution across patients, and association with replacement events suggest that alterations in *capD* provide a survival advantage for *S. aureus* on AD skin.

We did not detect comparably strong signals of adaptive *de novo* mutation across patients in *S. aureus* genes other than *capD*. Varying selective pressures across patients may have weakened adaptive signatures, and some adaptive events may have been removed by our strict filtering criteria (putative adaptive signatures, including mutations associated with sweeps, are listed in Table S4). In addition, although the presence of mobile elements varied across isolates in a lineage (Figure S8; Table S5), we did not find any selective sweep that was associated with the gain of a mobile element.

Capsule loss is common in AD globally

The polysaccharide capsule of *S. aureus* has been well studied, and it is generally considered a virulence factor that shields the pathogen from phagocytosis and the innate immune system.[36–38] However, the loss of the *S. aureus* capsule has been observed previously to emerge *in vitro* and *in vivo*,[39,40] and it has been shown that capsule-negative *S. aureus* exhibits improved adherence to fibrinogen, platelets, and endothelial cells.[41–43]

The adaptive emergence of *capD*-truncation mutations on AD skin suggests an advantage for the acapsular phenotype on AD skin.

We next sought to understand the generality of selection for *capD* alterations in our cohort. It is possible that replacement events involving *capD* emerged before the start of our study, given our inference of recent replacement events (Figure 2C). Alternatively, a patient's *S. aureus* population may have been initially founded by a strain with a nonfunctional *capD*. We tested all patient isolates for a complete *capD* open-reading frame and observed that the major lineage of four additional patients had ancestral truncation mutations in this gene. Three of these patients share the same frameshift mutation (single base insertion

CellPress
OPEN ACCESS

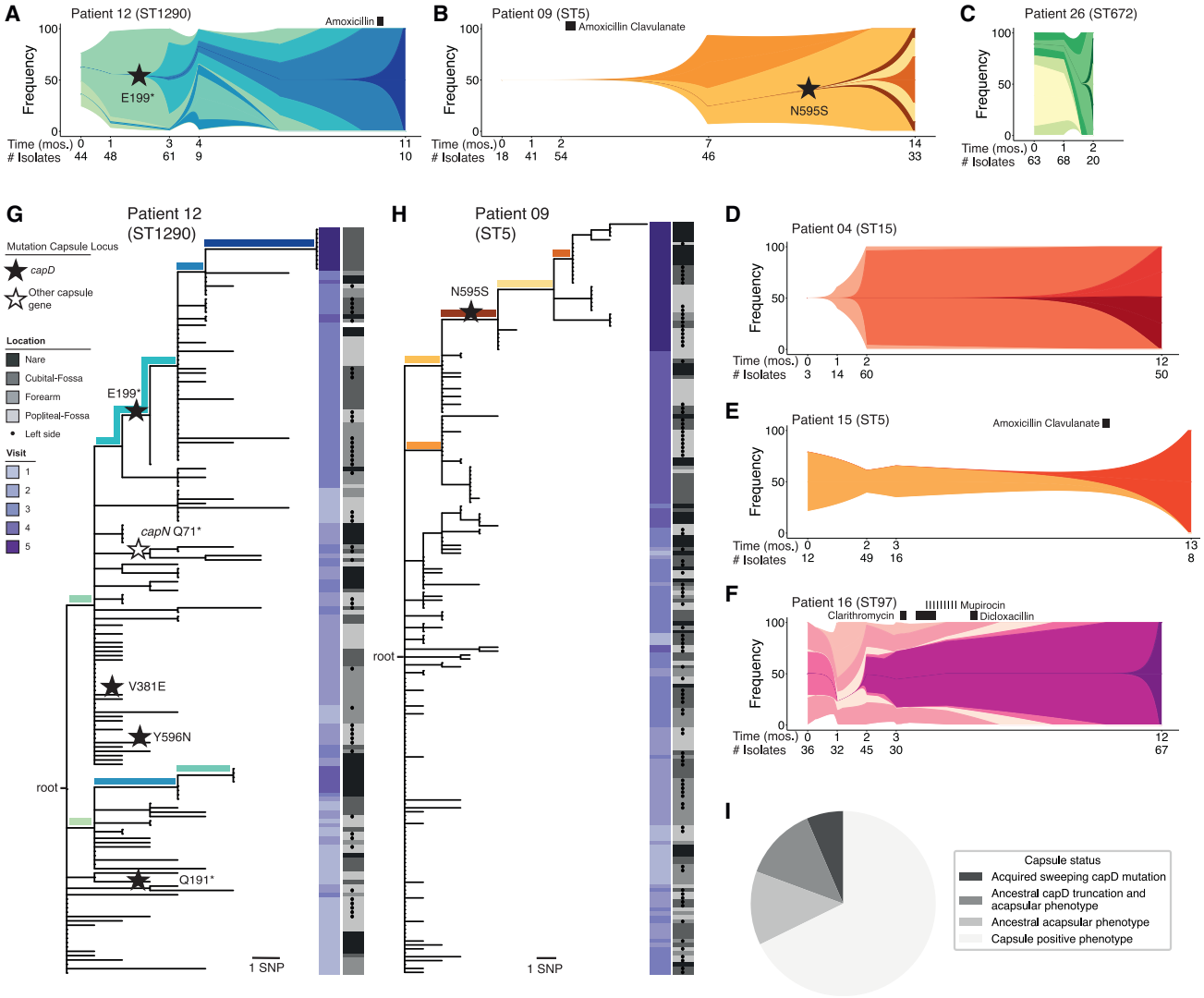

Figure 3. Rapid clonal spread of *de novo* mutations across the body implicates capsule loss as adaptive on treated AD skin

(A–F) Schematics representing the on-person evolution for all patients with ≥99 isolates, illustrating the emergence and occasional population-wide sweep of new genotypes. Each color represents a unique genotype found in at least 3 isolates and with a frequency shift of ≥30% for at least one visit. The shape and spacing of lines between time points with data are modeled based on exponential growth for maximum visibility and speculative (STAR Methods). Time points and number of isolates at each time point used for this modeling are indicated below the graph. A star indicates a mutation in *capD*; all other sweep-associated mutations are listed in Table S4. Black rectangles indicate time and duration of antibiotic treatment.

(G and H) Maximum parsimony tree of evolution of patient 12 (G) and patient 09 (H). The location from which each isolate was taken is indicated in gray (dots indicate left side of body), and time point is indicated by the purple heatmap. Stars indicate a mutation within the capsule locus. Branches representing mutations defining genotypes in (A) and (B) are colored accordingly. See Figures S5 and S6 for phylogenies of all other subjects.

(I) Pie chart indicating the capsule status for 31 major and minor lineages recovered from all 23 patients. Sweeping capsule mutations were observed in 2 patients' *S. aureus* populations, 4 lineages were determined genetically and by *in vitro* phenotyping to have lost the capsule before the start of our study, and 4 lineages were determined capsule-negative by *in vitro* phenotyping only (Table S3).

at an adenine hexamer of *capD*) also found in many CC8 strains, indicating that this mutation was carried on their founding strains. The remaining lineage had a unique *capD* truncation (10 bp deletion). We also searched for capsule loss driven by non-truncation mutations or mutations in other genes by performing immunoblots, which identified two additional major lineages without detectable polysaccharide capsules *in vitro*. In total, 6 of the 23 (26%) major lineages were acapsular at the time of enrollment (Figure 3I; Table S3), and 2 (12%) of the capsule-expressing major lineages acquired capD mutations during the course of the study.

To better understand whether the loss of *capD* is generally beneficial for *S. aureus in vivo* or specifically advantageous on AD skin, we leveraged publicly available genomes of isolates from people with and without AD. We analyzed 276 *S. aureus* isolate whole genomes from the skin of 110 AD patients, the nares of 67 healthy carriers, and the site of invasion of 99 individuals who had other infections (bloodstream, soft tissue, bones,

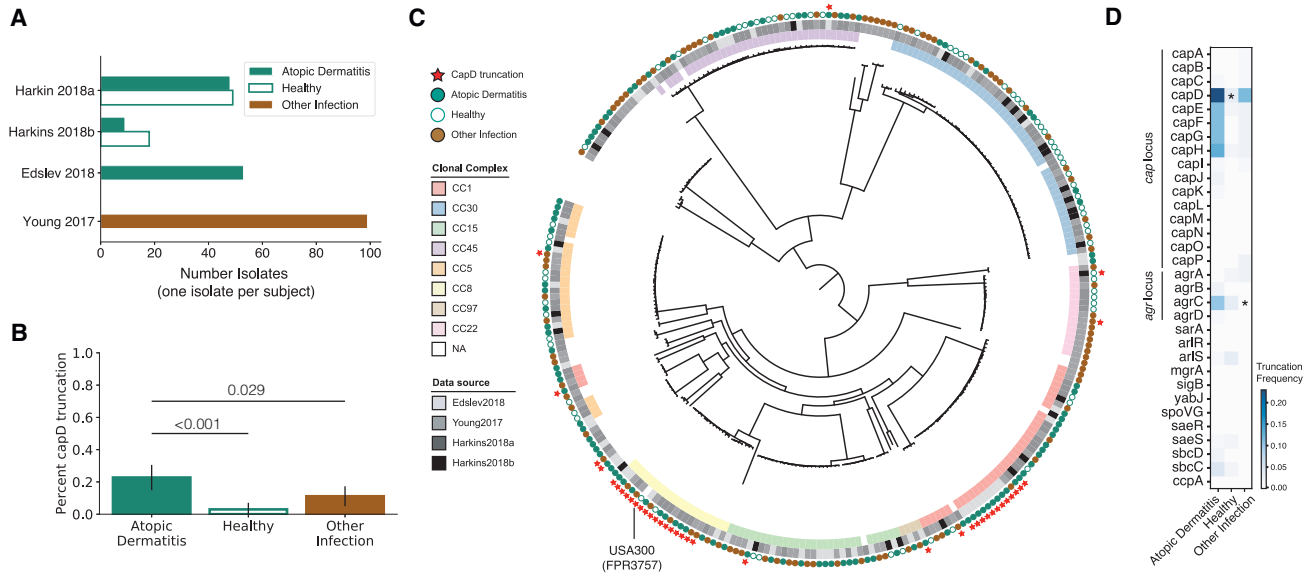

Figure 4. Meta-analysis of published data confirm enrichment of capsule loss on AD skin

(A) The number of *S. aureus* genomes downloaded from each of 4 public studies are shown.[25,44–46] Isolates were collected either from people with AD (green), the nares of healthy individuals (white), or from a variety of other diseases, including bloodstream, bone/joint, and soft-tissue infections (brown). When multiple isolates were available from a subject, only the isolate with the highest number of available reads was analyzed.

(B) The fraction of isolates with a truncated or missing *capD* is plotted as a function of isolation context. The 95% binomial proportion confidence interval is shown. P values are calculated using a one-sided Fisher's exact test.

(C) Phylogenetic tree showing relationship between all *S. aureus* analyzed, generated using a reference-based approach and maximum-likelihood reconstruction (STAR Methods). Isolates are labeled with squares indicating their membership in global clades and the study of origin, with circles indicating isolation context. Red stars indicate isolates without a full-length *capD*, showing 9 different independent occurrences including two expanded clades.

(D) Analysis similar to that in (B) was performed for other genes involved in capsule regulation, and the percentage of isolates from each context lacking a full-length copy of each gene is shown as a heatmap. *p < 0.001 vs. AD (one-sided Fisher's exact test). See Figures S9 and S10 for further analysis of the capsule locus and agrC loss

and joint; Figure 4A).[25,44–46] These samples were collected from individuals in Denmark, Ireland, and the United Kingdom.

Notably similar to our observation that 22% of AD patients carry a strain encoding a truncated CapD, 22.5% of AD-associated isolates in the public data lack a full-length *capD* gene. This represents a significant increase relative to isolates from healthy controls (7.2%, $p < 0.001$; one-sided Fisher's exact test) and from those with other types of infections (10.5%, $p = 0.020$) (Figure 4B). Phylogenetic analyses confirm several independent emergences of *capD* truncations, supporting the notion that *de novo* loss of *capD* can drive *S. aureus* adaptation (Figure 4C). Notably, 78% of capD-truncation isolates come from two independent, globally successful clones with recent expansions, including a CC8 clade from which USA300 is descended and a CC1 clade with a large deletion spanning *capD-capH*. The observation of this successful CC1 clade with capD loss is surprising in light of the known advantages of the capsule for immune evasion.[36–38] Nevertheless, the observed signal remains significant when isolates from CC8 are excluded (AD vs. healthy: $p < 0.001$, AD vs. other infection: $p = 0.016$) and when the entire dataset by Edslev et al.[45] is removed, which included most of the CC1-*capD*-negative isolates (AD vs. healthy $p = 0.014$). Furthermore, when considering all genes in the capsule locus, we observe an even stronger statistical enrichment of truncation mutations in isolates from AD ($p < 0.001$ vs. healthy; Figure S9A). These genomic differences indicate that selective pressures felt by *S. aureus* on AD skin are distinct from those in healthy patients or in the context of acute infection.

To understand whether capsule loss via mutations in other genes is also enriched in AD, we repeated the same analysis for genes known to be associated with capsule regulation.[47,48] Interestingly, *agrC*, the histidine-kinase sensor in the *agr* quorum-sensing-dependent virulence regulation system, also showed a significant enrichment of independent loss-of-function mutations in AD compared with other infections ($p < 0.001$) but not isolates from healthy patients (Figures 4D and S10). Although recent work has suggested that the retention of functional *agr* is associated with the onset of AD,[24] *agrA* loss has been previously documented on the skin of a patient with AD.[25] Loss of the *agr* system is known to suppress capsule production, among other virulence-associated pathways.[47,49] Although the selective advantage driving frequent *agr* loss in AD could be independent of the capsule, this observation is consistent with an advantage for an acapsular phenotype on AD skin.

What is the mechanistic basis of acapsular advantage on AD skin? Possible, non-mutually exclusive, selective pressures for capsule loss include: (1) immune escape from capsule-targeted antibodies or innate immune components, (2) increased adherence to AD skin via improved accessibility of surface adhesin proteins, and (3) alleviation of metabolic costs. Antibiotic resistance is unlikely to be a driver of capsule loss, as resistance-associated

genomic features were generally depleted from isolates from AD patients in our meta-analysis (Figures S9 and S11). The only antibiotic resistance enriched among isolates from AD patients was fusidic acid; we confirmed that its efficacy is not impacted by capsule negativity (Minimum inhibitory concentration 0.05 μg/mL for all strain pairs tested from Pt. 9 and Pt. 12; STAR Methods), and, therefore, its usage is not driving the association of capD and AD in the meta-analyses.

Metabolic costs may explain the preponderance of mutations in *capD*—the first gene in the biosynthetic pathway—rather than an even distribution across all capsule-associated genes. To understand the cost of capsule production, we measured growth rates in rich media and found that acapsular isolates grew 1.4%–2% faster than their capsular ancestors (an advantage amplified over multiple generations; Figure S12; STAR Methods). To test whether this growth advantage translated to better growth or worse disease *in vivo*, we compared the ability of these strains to cause skin injury in an mouse model that mimics an AD flare[50,51] and to colonize the unbroken skin of the mouse ear[8] (Figure S13; STAR Methods). This *in vitro* growth advantage of the acapsular strain did not translate to significantly worse disease or bacterial loads in these short-term models (<1 week). In addition, three AD isolates with point mutants that did not abrogate the capsule entirely did not show a growth advantage *in vitro* (Figure S12). Together, these data suggest additional selective pressures for the acapsular phenotype on AD skin that were not apparent in our mouse models, possibly due to the short duration of the *in vivo* experiment. The ability of acapsular strains to evade antibodies[52,53] and increase adhesion[41–43] have been demonstrated in mouse models of other infections and may play a role during long-term colonization on humans.

DISCUSSION

S. aureus is among the most successful opportunistic pathogens of humans, colonizing a third of the world's population, responsible for numerous outbreaks in healthcare facilities, and causing various acute and chronic diseases.[21] Here, we report that *S. aureus* rapidly adapts via *de novo* mutations on people being treated for AD, that adaptive mutants spread across the whole body—including the nares—and that loss-of-function mutations in an *S. aureus* gene closely associated with virulence, *capD*, are more frequent on the skin of people with AD than healthy controls.

Our findings of on-person adaptive evolution and association of capsule loss with AD are surprising, given the lack of a consistent signal between AD status and sequence types, clonal complexes, or other phylogenetic groupings[23]; this paradox is heightened by the observation that several global clades are already acapsular (e.g., USA300).[39] What is the cause of this discrepancy across genomic units? Possible explanations include selective tradeoffs,[54] person-specific selection,[55,56] and priority effects (advantage for early colonizers)[57] that limit the ability of any *S. aureus* clade to dominate across patients.[54] The possibility that such ecological factors dampen the signal for selection at the clade level raises the possibility that future studies with very large sample sizes powered for genome-wide analyses in the face of linkage[58] (see note in STAR Methods) may reveal additional *S. aureus* variations associated with AD and other diseases.

One question arising from this work is whether the advantage of *S. aureus* of being acapsular is specific to AD skin or translates to long-term skin colonization in general. Our data show that *S. aureus* isolates from AD patients are more often acapsular than those from infection or healthy nares, but we are unable to acquire a large number of genomes derived from the skin of people without AD for comparison. Although the acapsular USA300 clade is known to spread between healthy individuals,[39] it remains to be determined whether USA300's acapsularity is beneficial for its spread or survival or plays only a minor role, given the other advantages that this clade has for colonization of nares.[59] Regardless, our in-human results suggest that acapsular strains may be harder to remove from AD skin than capsular strains, and long-term colonization may raise the risk of strains with such phenotypes emerging.

Future work might combine small molecules or other therapies that specifically target *S. aureus* strains without a functional capsule locus with selective forces on the host to lower the burden of *S. aureus* colonization in AD. Further characterization of the mechanistic basis behind the CapD-negative advantage on AD skin (or skin in general) will be critical to the design of any such therapies, as unexpected consequences may emerge from selection for the capsular phenotype, which is more virulent in other disease contexts.[36,60]

This study focused on *S. aureus* genotypes that could be easily recovered from swabs at 7 body sites from 23 people. Given the relatively small sample size of our cohort and other sources of disease severity variation, including host genetic variation and treatment, we were unable to directly associate *S. aureus capD* status with AD severity or duration. Similarly, we were unable to study the impact of specific treatment variation on sweeping patterns or capsule status, although we note that lineage-wide sweeps and the acquisition of mutations in the capsule locus were both observed in patients who did and did not receive bleach baths (Figures 3A–3F; Table S1). We did not seek to characterize community members at low abundance, and it is possible that additional minority lineages and genotypes were present at undetected levels or additional locations on the body (Figures S14 and S15). Similar limitations exist for culture-independent approaches, as it is difficult to distinguish between sample cross-contamination and low abundance colonization.[61] Our data indeed support a model in which lineages can persistently colonize despite lack of detection; we recover the exact same lineages from four patients after visits at which no *S. aureus* was recovered (Figure 1B). Notwithstanding, we find no cases of within-lineage reemergence of replaced genotypes, supporting the durability of observed intralineage sweeps on the skin of people treated with AD. As all patients were treated for AD, additional work is needed to test whether *S. aureus* has similar dynamics in untreated AD and to understand the specific contribution of treatment, and its resultant decrease in population size,[62] on *S. aureus* on-person evolutionary dynamics.

Together, our results highlight the potential of *de novo* mutations for altering bacterial competitiveness in microbiomes, highlight the power of mutation tracking for identifying new potential therapeutic directions, and suggest that whole-genome resolution may be required for predicting the impact of microbial strains on complex diseases.

STAR★METHODS

Detailed methods are provided in the online version of this paper and include the following:

- KEY RESOURCES TABLE
- RESOURCE AVAILABILITY
  - Lead contact
  - Materials availability
  - Data and code availability
- EXPERIMENTAL MODEL AND SUBJECT DETAILS
  - Study cohort and sample collection
- METHOD DETAILS
  - Culturing and single-colony sequencing
  - Assignment of isolates to lineages
  - Within-patient phylogenetic reconstruction
  - Molecular clock and TMRCA
  - Signatures of on-person adaptive evolution
  - Creation of Muller plots
  - Mobile genetic element analysis
  - Capsule typing
  - Growth rate
  - Fusidic acid susceptibility
  - Public *S. aureus* isolate genome analysis
  - *in vivo* infection models
  - Collectors curve analysis
- QUANTIFICATION AND STATISTICAL ANALYSIS

SUPPLEMENTAL INFORMATION

Supplemental information can be found online at https://doi.org/10.1016/j.chom.2023.03.009.

ACKNOWLEDGMENTS

We thank Mariana Matus and Eric Alm for assistance in the design of the clinical cohort, the BioMicroCenter at MIT for performing genomic sequencing, Adrián Martínez-Gayosso and Blanca L. Campos-Cabrera for assistance with patient sampling, Armando Jerónimo-Gallegos for assistance with colony preparation, Samantha Choi for technical support on animal experiments, Paul F. Koffi for performing *in vitro* capsule immunoblots, Chris Manusco and Calen Mendall for experimental assistance, and members of the Lieberman lab for valuable advice and feedback on the manuscript. We acknowledge support from MISTI Global Seed Funds (to T.D.L. and M.T.G.-R.), the National Institutes of Health (DP2-GM140922 to T.D.L., R01AI30019 to I.M.C.), Burroughs Wellcome Fund (to I.M.C.), the Mexican Government Ministry of Taxes Program E022 for Health Research and Technological Development 2018 (to M.T.G.-R.), and DFG research fellowship (KE 2408/1-1 to F.M.K.).

AUTHOR CONTRIBUTIONS

M.T.G.-R. and T.D.L. designed the clinical cohort. M.T.G.-R. enrolled patients and collected clinical samples. C.R.-G. cultured bacteria from clinical samples and extracted DNA. T.C.L. and T.D.L. prepared genomic libraries. F.M.K. and T.D.L. performed genomic analysis and interpretation. J.C.L. performed capsule assays and provided *S. aureus* strains. V.D.K. and L.D. performed *in vitro* experiments. V.D.K., K.J.B., L.D., and I.M.C. performed mouse experiments. F.M.K. and T.D.L. wrote the manuscript with feedback from all authors.

DECLARATION OF INTERESTS

The lab of T.D.L. has received funding from Colgate PalmOlive for studies following this work. The lab of I.M.C. has received sponsored research work from Abbvie pharmaceuticals.

Received: September 25, 2022
Revised: February 14, 2023
Accepted: March 10, 2023
Published: April 6, 2023

REFERENCES

1. Lieberman, T.D., Michel, J.B., Aingaran, M., Potter-Bynoe, G., Roux, D., Davis, M.R., Jr., Skurnik, D., Leiby, N., LiPuma, J.J., Goldberg, J.B., et al. (2011). Parallel bacterial evolution within multiple patients identifies candidate pathogenicity genes. Nat. Genet. *43*, 1275–1280. https://doi.org/10.1038/ng.997.
2. Snitkin, E.S., Zelazny, A.M., Gupta, J., Nisc Comparative Sequencing Program, Palmore, T.N., Murray, P.R., and Segre, J.A. (2013). Genomic insights into the fate of colistin resistance and Acinetobacter baumannii during patient treatment. Genome Res. *23*, 1155–1162. https://doi.org/10.1101/gr.154328.112.
3. Ernst, C.M., Braxton, J.R., Rodriguez-Osorio, C.A., Zagieboylo, A.P., Li, L., Pironti, A., Manson, A.L., Nair, A.V., Benson, M., and Cummins, K. (2020). Adaptive evolution of virulence and persistence in carbapenem-resistant Klebsiella pneumoniae. Nat. Med. *26*, 705–711.
4. Zhao, S., Lieberman, T.D., Poyet, M., Kauffman, K.M., Gibbons, S.M., Groussin, M., Xavier, R.J., and Alm, E.J. (2019). Adaptive evolution within gut microbiomes of healthy people. Cell Host Microbe *25*, 656–667.e8.
5. Williams, M.R., and Gallo, R.L. (2015). The role of the skin microbiome in atopic dermatitis. Curr. Allergy Asthma Rep. *15*, 65. https://doi.org/10.1007/s11882-015-0567-4.
6. Ni, J., Wu, G.D., Albenberg, L., and Tomov, V.T. (2017). Gut microbiota and IBD: causation or correlation? Nat. Rev. Gastroenterol. Hepatol. *14*, 573–584.
7. Nakatsuji, T., Chen, T.H., Narala, S., Chun, K.A., Two, A.M., Yun, T., Shafiq, F., Kotol, P.F., Bouslimani, A., and Melnik, A.V. (2017). Antimicrobials from human skin commensal bacteria protect against Staphylococcus aureus and are deficient in atopic dermatitis. Sci. Transl. Med. *9*, eaah4680.
8. Byrd, A.L., Deming, C., Cassidy, S.K.B., Harrison, O.J., Ng, W.I., Conlan, S., NISC Comparative Sequencing Program, Belkaid, Y., Segre, J.A., and Kong, H.H. (2017). Staphylococcus aureus and Staphylococcus epidermidis strain diversity underlying pediatric atopic dermatitis. Sci. Transl. Med. *9*, eaal4651.
9. Hall, A.B., Yassour, M., Sauk, J., Garner, A., Jiang, X., Arthur, T., Lagoudas, G.K., Vatanen, T., Fornelos, N., Wilson, R., et al. (2017). A novel Ruminococcus gnavus clade enriched in inflammatory bowel disease patients. Genome Med. *9*, 103. https://doi.org/10.1186/s13073-017-0490-5.
10. Asher, M.I., Montefort, S., Björkstén, B., Lai, C.K.W., Strachan, D.P., Weiland, S.K., and Williams, H.; ISAAC Phase Three Study Group (2006). Worldwide time trends in the prevalence of symptoms of asthma, allergic rhinoconjunctivitis, and eczema in childhood: ISAAC Phases One and Three repeat multicountry cross-sectional surveys. Lancet *368*, 733–743. https://doi.org/10.1016/S0140-6736(06)69283-0.
11. Hay, R.J., Johns, N.E., Williams, H.C., Bolliger, I.W., Dellavalle, R.P., Margolis, D.J., Marks, R., Naldi, L., Weinstock, M.A., Wulf, S.K., et al. (2014). The global burden of skin disease in 2010: an analysis of the prevalence and impact of skin conditions. J. Invest. Dermatol. *134*, 1527–1534. https://doi.org/10.1038/jid.2013.446.
12. Baurecht, H., Rühlemann, M.C., Rodríguez, E., Thielking, F., Harder, I., Erkens, A.S., Stölzl, D., Ellinghaus, E., Hotze, M., Lieb, W., et al. (2018). Epidermal lipid composition, barrier integrity, and eczematous inflammation are associated with skin microbiome configuration. J. Allergy Clin. Immunol. *141*, 1668–1676.e16. https://doi.org/10.1016/j.jaci.2018.01.019.
13. Leyden, J.J., Marples, R.R., and Kligman, A.M. (1974). Staphylococcus aureus in the lesions of atopic dermatitis. Br. J. Dermatol. *90*, 525–530. https://doi.org/10.1111/j.1365-2133.1974.tb06447.x.

14. Kong, H.H., Oh, J., Deming, C., Conlan, S., Grice, E.A., Beatson, M.A., Nomicos, E., Polley, E.C., Komarow, H.D., et al.; Nisc Comparative Sequence Program (2012). Temporal shifts in the skin microbiome associated with disease flares and treatment in children with atopic dermatitis. Genome Res. *22*, 850–859.

15. Tauber, M., Balica, S., Hsu, C.-Y., Jean-Decoster, C., Lauze, C., Redoules, D., Viodé, C., Schmitt, A.-M., Serre, G., and Simon, M. (2016). Staphylococcus aureus density on lesional and nonlesional skin is strongly associated with disease severity in atopic dermatitis. J. Allergy Clin. Immunol. *137*, 1272–1274.e3.

16. Huang, J.T., Abrams, M., Tlougan, B., Rademaker, A., and Paller, A.S. (2009). Treatment of Staphylococcus aureus colonization in atopic dermatitis decreases disease severity. Pediatrics *123*, e808–e814.

17. Paller, A.S., Kong, H.H., Seed, P., Naik, S., Scharschmidt, T.C., Gallo, R.L., Luger, T., and Irvine, A.D. (2019). The microbiome in patients with atopic dermatitis. J. Allergy Clin. Immunol. *143*, 26–35. https://doi.org/10.1016/j.jaci.2018.11.015.

18. Khadka, V.D., Key, F.M., Romo-González, C., Martínez-Gayosso, A., Campos-Cabrera, B.L., Gerónimo-Gallegos, A., Lynn, T.C., Durán-McKinster, C., Coria-Jiménez, R., Lieberman, T.D., et al. (2021). The skin microbiome of patients with atopic dermatitis normalizes gradually during treatment. Front. Cell. Infect. Microbiol. *11*, 720674. https://doi.org/10.3389/fcimb.2021.720674.

19. Gorwitz, R.J., Kruszon-Moran, D., McAllister, S.K., McQuillan, G., McDougal, L.K., Fosheim, G.E., Jensen, B.J., Killgore, G., Tenover, F.C., and Kuehnert, M.J. (2008). Changes in the prevalence of nasal colonization with Staphylococcus aureus in the United States, 2001–2004. J. Infect. Dis. *197*, 1226–1234. https://doi.org/10.1086/533494.

20. Oh, J., Byrd, A.L., Deming, C., Conlan, S., NISC Comparative Sequencing Program, Kong, H.H., and Segre, J.A. (2014). Biogeography and individuality shape function in the human skin metagenome. Nature *514*, 59–64. https://doi.org/10.1038/nature13786.

21. Tong, S.Y.C., Davis, J.S., Eichenberger, E., Holland, T.L., and Fowler, V.G. (2015). Staphylococcus aureus infections: epidemiology, pathophysiology, clinical manifestations, and management. Clin. Microbiol. Rev. *28*, 603–661. https://doi.org/10.1128/CMR.00134-14.

22. Enright, M.C., Robinson, D.A., Randle, G., Feil, E.J., Grundmann, H., and Spratt, B.G. (2002). The evolutionary history of methicillin-resistant Staphylococcus aureus (MRSA). Proc. Natl. Acad. Sci. USA *99*, 7687–7692.

23. Ogonowska, P., Gilaberte, Y., Barańska-Rybak, W., and Nakonieczna, J. (2020). Colonization with Staphylococcus aureus in atopic dermatitis patients: attempts to reveal the unknown. Front. Microbiol. *11*, 567090. https://doi.org/10.3389/fmicb.2020.567090.

24. Nakamura, Y., Takahashi, H., Takaya, A., Inoue, Y., Katayama, Y., Kusuya, Y., Shoji, T., Takada, S., Nakagawa, S., Oguma, R., et al. (2020). Staphylococcus Agr virulence is critical for epidermal colonization and associates with atopic dermatitis development. Sci. Transl. Med. *12*, eaay4068. https://doi.org/10.1126/scitranslmed.aay4068.

25. Harkins, C.P., Pettigrew, K.A., Oravcová, K., Gardner, J., Hearn, R.M.R., Rice, D., Mather, A.E., Parkhill, J., Brown, S.J., Proby, C.M., et al. (2018). The microevolution and epidemiology of Staphylococcus aureus colonization during atopic eczema disease flare. J. Invest. Dermatol. *138*, 336–343. https://doi.org/10.1016/j.jid.2017.09.023.

26. Chopra, R., Vakharia, P.P., Sacotte, R., Patel, N., Immaneni, S., White, T., Kantor, R., Hsu, D.Y., and Silverberg, J.I. (2017). Severity strata for Eczema Area and Severity Index (EASI), modified EASI, Scoring Atopic Dermatitis (SCORAD), objective SCORAD, Atopic Dermatitis Severity Index and body surface area in adolescents and adults with atopic dermatitis. Br. J. Dermatol. *177*, 1316–1321.

27. Holden, M.T., Hsu, L.Y., Kurt, K., Weinert, L.A., Mather, A.E., Harris, S.R., Strommenger, B., Layer, F., Witte, W., de Lencastre, H., et al. (2013). A genomic portrait of the emergence, evolution, and global spread of a methicillin-resistant Staphylococcus aureus pandemic. Genome Res. *23*, 653–664. https://doi.org/10.1101/gr.147710.112.

28. McAdam, P.R., Templeton, K.E., Edwards, G.F., Holden, M.T.G., Feil, E.J., Aanensen, D.M., Bargawi, H.J.A., Spratt, B.G., Bentley, S.D., Parkhill, J., et al. (2012). Molecular tracing of the emergence, adaptation, and transmission of hospital-associated methicillin-resistant Staphylococcus aureus. Proc. Natl. Acad. Sci. USA *109*, 9107–9112. https://doi.org/10.1073/pnas.1202869109.

29. Nübel, U., Nachtnebel, M., Falkenhorst, G., Benzler, J., Hecht, J., Kube, M., Bröcker, F., Moelling, K., Bührer, C., Gastmeier, P., et al. (2013). MRSA transmission on a Neonatal Intensive Care Unit: epidemiological and genome-based phylogenetic analyses. PLoS One *8*, e54898. https://doi.org/10.1371/journal.pone.0054898.

30. Uhlemann, A.C., Dordel, J., Knox, J.R., Raven, K.E., Parkhill, J., Holden, M.T., Peacock, S.J., and Lowy, F.D. (2014). Molecular tracing of the emergence, diversification, and transmission of S. aureus sequence type 8 in a New York community. Proc. Natl. Acad. Sci. USA *111*, 6738–6743. https://doi.org/10.1073/pnas.1401006111.

31. Young, B.C., Golubchik, T., Batty, E.M., Fung, R., Larner-Svensson, H., Votintseva, A.A., Miller, R.R., Godwin, H., Knox, K., Everitt, R.G., et al. (2012). Evolutionary dynamics of Staphylococcus aureus during progression from carriage to disease. Proc. Natl. Acad. Sci. USA *109*, 4550–4555. https://doi.org/10.1073/pnas.1113219109.

32. Golubchik, T., Batty, E.M., Miller, R.R., Farr, H., Young, B.C., Larner-Svensson, H., Fung, R., Godwin, H., Knox, K., Votintseva, A., et al. (2013). Within-host evolution of Staphylococcus aureus during asymptomatic carriage. PLoS One *8*, e61319. https://doi.org/10.1371/journal.pone.0061319.

33. Turner, N.A., Sharma-Kuinkel, B.K., Maskarinec, S.A., Eichenberger, E.M., Shah, P.P., Carugati, M., Holland, T.L., and Fowler, V.G. (2019). Methicillin-resistant Staphylococcus aureus: an overview of basic and clinical research. Nat. Rev. Microbiol. *17*, 203–218.

34. Lieberman, T.D., Flett, K.B., Yelin, I., Martin, T.R., McAdam, A.J., Priebe, G.P., and Kishony, R. (2014). Genetic variation of a bacterial pathogen within individuals with cystic fibrosis provides a record of selective pressures. Nat. Genet. *46*, 82–87. https://doi.org/10.1038/ng.2848.

35. Nguyen, D., and Singh, P.K. (2006). Evolving stealth: genetic adaptation of Pseudomonas aeruginosa during cystic fibrosis infections. Proc. Natl. Acad. Sci. USA *103*, 8305–8306. https://doi.org/10.1073/pnas.0602526103.

36. O'Riordan, K., and Lee, J.C. (2004). Staphylococcus aureus capsular polysaccharides. Clin. Microbiol. Rev. *17*, 218–234.

37. Kuipers, A., Stapels, D.A.C., Weerwind, L.T., Ko, Y.-P., Ruyken, M., Lee, J.C., van Kessel, K.P.M., and Rooijakkers, S.H.M. (2016). The Staphylococcus aureus polysaccharide capsule and Efb-dependent fibrinogen shield act in concert to protect against phagocytosis. Microbiology *162*, 1185–1194.

38. Verbrugh, H.A., Peterson, P.K., Nguyen, B.Y., Sisson, S.P., and Kim, Y. (1982). Opsonization of encapsulated Staphylococcus aureus: the role of specific antibody and complement. J. Immunol. *129*, 1681–1687.

39. Boyle-Vavra, S., Li, X., Alam, M.T., Read, T.D., Sieth, J., Cywes-Bentley, C., Dobbins, G., David, M.Z., Kumar, N., Eells, S.J., et al. (2015). USA300 and USA500 clonal lineages of Staphylococcus aureus do not produce a capsular polysaccharide due to conserved mutations in the cap5 locus. mBio *6*. e02585–e02514. https://doi.org/10.1128/mBio.02585-14.

40. Mohamed, N., Timofeyeva, Y., Jamrozy, D., Rojas, E., Hao, L., Silmon de Monerri, N.C., Hawkins, J., Singh, G., Cai, B., Liberator, P., et al. (2019). Molecular epidemiology and expression of capsular polysaccharides in Staphylococcus aureus clinical isolates in the United States. PLoS One *14*, e0208356. https://doi.org/10.1371/journal.pone.0208356.

41. Pöhlmann-Dietze, P., Ulrich, M., Kiser, K.B., Döring, G., Lee, J.C., Fournier, J.M., Botzenhart, K., and Wolz, C. (2000). Adherence of Staphylococcus aureus to endothelial cells: influence of capsular polysaccharide, global regulator agr, and bacterial growth phase. Infect. Immun. *68*, 4865–4871. https://doi.org/10.1128/IAI.68.9.4865-4871.2000.

42. Risley, A.L., Loughman, A., Cywes-Bentley, C., Foster, T.J., and Lee, J.C. (2007). Capsular polysaccharide masks clumping factor A-mediated adherence of Staphylococcus aureus to fibrinogen and platelets. J. Infect. Dis. *196*, 919–927. https://doi.org/10.1086/520932.

43. Tuchscherr, L.P., Buzzola, F.R., Alvarez, L.P., Caccuri, R.L., Lee, J.C., and Sordelli, D.O. (2005). Capsule-negative Staphylococcus aureus induces chronic experimental mastitis in mice. Infect. Immun. *73*, 7932–7937. https://doi.org/10.1128/IAI.73.12.7932-7937.2005.

44. Young, B.C., Wu, C.-H., Gordon, N.C., Cole, K., Price, J.R., Liu, E., Sheppard, A.E., Perera, S., Charlesworth, J., and Golubchik, T. (2017). Severe infections emerge from commensal bacteria by adaptive evolution. eLife *6*, e30637.

45. Edslev, S.M., Clausen, M.-L., Agner, T., Stegger, M., and Andersen, P.S. (2018). Genomic analysis reveals different mechanisms of fusidic acid resistance in Staphylococcus aureus from Danish atopic dermatitis patients. J. Antimicrob. Chemother. *73*, 856–861.

46. Harkins, C.P., McAleer, M.A., Bennett, D., McHugh, M., Fleury, O.M., Pettigrew, K.A., Oravcová, K., Parkhill, J., Proby, C.M., Dawe, R.S., et al. (2018). The widespread use of topical antimicrobials enriches for resistance in Staphylococcus aureus isolated from patients with atopic dermatitis. Br. J. Dermatol. *179*, 951–958. https://doi.org/10.1111/bjd.16722.

47. Lei, M.G., and Lee, C.Y. (2020). MgrA activates staphylococcal capsule via SigA-dependent promoter. J. Bacteriol. *203*, e00495–20. https://doi.org/10.1128/JB.00495-20.

48. Keinhörster, D., George, S.E., Weidenmaier, C., and Wolz, C. (2019). Function and regulation of Staphylococcus aureus wall teichoic acids and capsular polysaccharides. Int. J. Med. Microbiol. *309*, 151333. https://doi.org/10.1016/j.ijmm.2019.151333.

49. Luong, T., Sau, S., Gomez, M., Lee, J.C., and Lee, C.Y. (2002). Regulation of Staphylococcus aureus capsular polysaccharide expression by agr and sarA. Infect. Immun. *70*, 444–450.

50. Nakamura, Y., Oscherwitz, J., Cease, K.B., Chan, S.M., Muñoz-Planillo, R., Hasegawa, M., Villaruz, A.E., Cheung, G.Y.C., McGavin, M.J., Travers, J.B., et al. (2013). Staphylococcus δ-toxin induces allergic skin disease by activating mast cells. Nature *503*, 397–401. https://doi.org/10.1038/nature12655.

51. Nakagawa, S., Matsumoto, M., Katayama, Y., Oguma, R., Wakabayashi, S., Nygaard, T., Saijo, S., Inohara, N., Otto, M., Matsue, H., et al. (2017). Staphylococcus aureus virulent PSMα peptides induce keratinocyte alarmin release to orchestrate IL-17-dependent skin inflammation. Cell Host Microbe *22*, 667–677.e5. https://doi.org/10.1016/j.chom.2017.10.008.

52. Shinefield, H., Black, S., Fattom, A., Horwith, G., Rasgon, S., Ordonez, J., Yeoh, H., Law, D., Robbins, J.B., Schneerson, R., et al. (2002). Use of a Staphylococcus aureus conjugate vaccine in patients receiving hemodialysis. N. Engl. J. Med. *346*, 491–496. https://doi.org/10.1056/NEJMoa011297.

53. Tuchscherr, L.P.N., Buzzola, F.R., Alvarez, L.P., Lee, J.C., and Sordelli, D.O. (2008). Antibodies to capsular polysaccharide and clumping Factor A prevent mastitis and the emergence of unencapsulated and small-colony variants of *Staphylococcus aureus* in mice. Infect. Immun. *76*, 5738–5744. https://doi.org/10.1128/IAI.00874-08.

54. Culyba, M.J., and Van Tyne, D. (2021). Bacterial evolution during human infection: adapt and live or adapt and die. PLoS Pathog. *17*, e1009872. https://doi.org/10.1371/journal.ppat.1009872.

55. Zdziarski, J., Brzuszkiewicz, E., Wullt, B., Liesegang, H., Biran, D., Voigt, B., Grönberg-Hernandez, J., Ragnarsdottir, B., Hecker, M., Ron, E.Z., et al. (2010). host imprints on bacterial genomes—rapid, divergent evolution in individual patients. PLoS Pathog. *6*, e1001078. https://doi.org/10.1371/journal.ppat.1001078.

56. Elhenawy, W., Tsai, C.N., and Coombes, B.K. (2019). Host-Specific Adaptive Diversification of Crohn's Disease-Associated Adherent-Invasive Escherichia coli. Cell Host Microbe *25*, 301–312.e5. https://doi.org/10.1016/j.chom.2018.12.010.

57. Debray, R., Herbert, R.A., Jaffe, A.L., Crits-Christoph, A., Power, M.E., and Koskella, B. (2022). Priority effects in microbiome assembly. Nat. Rev. Microbiol. *20*, 109–121. https://doi.org/10.1038/s41579-021-00604-w.

58. Collins, C., and Didelot, X. (2018). A phylogenetic method to perform genome-wide association studies in microbes that accounts for population structure and recombination. PLoS Comput. Biol. *14*, e1005958. https://doi.org/10.1371/journal.pcbi.1005958.

59. Thurlow, L.R., Joshi, G.S., and Richardson, A.R. (2012). Virulence strategies of the dominant USA300 lineage of community-associated methicillin-resistant Staphylococcus aureus (CA-MRSA). FEMS Immunol. Med. Microbiol. *65*, 5–22. https://doi.org/10.1111/j.1574-695X.2012.00937.x.

60. Suligoy, C.M., Díaz, R.E., Gehrke, A.K., Ring, N., Yebra, G., Alves, J., Gómez, M.I., Wendler, S., Fitzgerald, J.R., Tuchscherr, L., et al. (2020). Acapsular Staphylococcus aureus with a non-functional agr regains capsule expression after passage through the bloodstream in a bacteremia mouse model. Sci. Rep. *10*, 14108. https://doi.org/10.1038/s41598-020-70671-1.

61. Lou, Y.C., Hoff, J., Olm, M.R., West-Roberts, J., Diamond, S., Firek, B.A., Morowitz, M.J., and Banfield, J.F. (2022). Using strain-resolved analysis to identify contamination in metagenomics data. Preprint at bioRxiv. https://doi.org/10.1101/2022.01.16.476537.

62. Hauser, C., Wuethrich, B., Matter, L., Wilhelm, J.A., Sonnabend, W., and Schopfer, K. (1985). *Staphylococcus aureus* skin colonization in atopic dermatitis patients. Dermatologica *170*, 35–39. https://doi.org/10.1159/000249493.

63. Tollersrud, T., Kenny, K., Reitz, A.J., Jr., and Lee, J.C. (2000). Genetic and serologic evaluation of capsule production by bovine mammary isolates of Staphylococcus aureus and other Staphylococcus spp. from Europe and the United States. J. Clin. Microbiol. *38*, 2998–3003.

64. Mölder, F., Jablonski, K.P., Letcher, B., Hall, M.B., Tomkins-Tinch, C.H., Sochat, V., Forster, J., Lee, S., Twardziok, S.O., Kanitz, A., et al. (2021). Sustainable data analysis with Snakemake [version 1; peer review: 1 approved, 1 approved with reservations]. F1000Res *10*, 33. https://doi.org/10.12688/f1000research.29032.2.

65. Joshi, N.A., and Fass, J.N. (2011). Sickle: a sliding-window, adaptive, quality-based trimming tool for FastQ files. https://github.com/najoshi/sickle.

66. Langmead, B., and Salzberg, S.L. (2012). Fast gapped-read alignment with Bowtie 2. Nat. Methods *9*, 357–359.

67. Danecek, P., Bonfield, J.K., Liddle, J., Marshall, J., Ohan, V., Pollard, M.O., Whitwham, A., Keane, T., McCarthy, S.A., Davies, R.M., et al. (2021). Twelve years of SAMtools and BCFtools. GigaScience *10*, giab008.

68. Wood, D.E., Lu, J., and Langmead, B. (2019). Improved metagenomic analysis with Kraken 2. Genome Biol. *20*, 257.

69. Felsenstein, J. PHYLIP (phylogeny inference package). 2005. Distributed by the author. Seattle: Department of Genome Sciences, University of Washington. https://evolution.genetics.washington.edu/phylip.html.

70. Bankevich, A., Nurk, S., Antipov, D., Gurevich, A.A., Dvorkin, M., Kulikov, A.S., Lesin, V.M., Nikolenko, S.I., Pham, S., Prjibelski, A.D., et al. (2012). SPAdes: a new genome assembly algorithm and its applications to single-cell sequencing. J. Comput. Biol. *19*, 455–477. https://doi.org/10.1089/cmb.2012.0021.

71. Seemann, T. (2014). Prokka: rapid prokaryotic genome annotation. Bioinformatics *30*, 2068–2069. https://doi.org/10.1093/bioinformatics/btu153.

72. Fu, L., Niu, B., Zhu, Z., Wu, S., and Li, W. (2012). CD-HIT: accelerated for clustering the next-generation sequencing data. Bioinformatics *28*, 3150–3152.

73. Sagulenko, P., Puller, V., and Neher, R.A. (2018). TreeTime: maximum-likelihood phylodynamic analysis. Virus Evol. *4*, vex042. https://doi.org/10.1093/ve/vex042.

74. Inouye, M., Dashnow, H., Raven, L.-A., Schultz, M.B., Pope, B.J., Tomita, T., Zobel, J., and Holt, K.E. (2014). SRST2: rapid genomic surveillance for

public health and hospital microbiology labs. Genome Med. *6*, 90. https://doi.org/10.1186/s13073-014-0090-6.

75. Hanifin, J.M. (1980). Diagnostic features of atopic dermatitis. Acta Derm. Venereol. *92*, 44–47.
76. Baym, M., Kryazhimskiy, S., Lieberman, T.D., Chung, H., Desai, M.M., and Kishony, R. (2015). Inexpensive multiplexed library preparation for megabase-sized genomes. PLOS One *10*, e0128036. https://doi.org/10.1371/journal.pone.0128036.
77. Martin, M. (2011). Cutadapt removes adapter sequences from high-throughput sequencing reads. EMBnet J. *17*, 10–12.
78. Li, H., and Durbin, R. (2009). Fast and accurate short read alignment with Burrows–Wheeler transform. Bioinformatics *25*, 1754–1760. https://doi.org/10.1093/bioinformatics/btp324.
79. Stamatakis, A. (2014). RAxML version 8: a tool for phylogenetic analysis and post-analysis of large phylogenies. Bioinformatics *30*, 1312–1313. https://doi.org/10.1093/bioinformatics/btu033.
80. Letunic, I., and Bork, P. (2021). Interactive Tree Of Life (iTOL) v5: an online tool for phylogenetic tree display and annotation. Nucleic Acids Res. *49*, W293–W296.
81. Jolley, K.A., Bray, J.E., and Maiden, M.C.J. (2018). Open-access bacterial population genomics: BIGSdb software, the website and their applications.PubMLST.orgPubMLST.org. Wellcome Open Res. *3*, 124. https://doi.org/10.12688/wellcomeopenres.14826.1.
82. Singh, M., Sasaki, T., Matsuo, M., Morimoto, Y., Aiba, Y., and Hiramatsu, K. (2015). Complete genome sequence of the drug-naive classical Staphylococcus aureus strain FDA209P. Genome Announc. *3*. e01343–e01315.
83. Virtanen, P., Gommers, R., Oliphant, T.E., Haberland, M., Reddy, T., Cournapeau, D., Burovski, E., Peterson, P., Weckesser, W., Bright, J., et al. (2020). SciPy 1.0: fundamental algorithms for scientific computing in Python. Nat. Methods *17*, 261–272. https://doi.org/10.1038/s41592-019-0686-2.
84. Pritchard, J.K., Pickrell, J.K., and Coop, G. (2010). The genetics of human adaptation: hard sweeps, soft sweeps, and polygenic adaptation. Curr. Biol. *20*, R208–R215. https://doi.org/10.1016/j.cub.2009.11.055.
85. Garud, N.R., Good, B.H., Hallatschek, O., and Pollard, K.S. (2019). Evolutionary dynamics of bacteria in the gut microbiome within and across hosts. PLoS Biol. *17*, e3000102.
86. Lang, G.I., Botstein, D., and Desai, M.M. (2011). Genetic variation and the fate of beneficial mutations in asexual populations. Genetics *188*, 647–661.
87. Conwill, A., Kuan, A.C., Damerla, R., Poret, A.J., Baker, J.S., Tripp, A.D., Alm, E.J., and Lieberman, T.D. (2022). Anatomy promotes neutral coexistence of strains in the human skin microbiome. Cell Host Microbe *30*, 171–182.e7. https://doi.org/10.1016/j.chom.2021.12.007.
88. Noble, R. (2019). Ggmuller: Create Muller Plots of Evolutionary Dynamics.
89. Lee, J.C., Liu, M.J., Parsonnet, J., and Arbeit, R.D. (1990). Expression of type 8 capsular polysaccharide and production of toxic shock syndrome toxin 1 are associated among vaginal isolates of Staphylococcus aureus. J. Clin. Microbiol. *28*, 2612–2615.
90. Madden, T. (2013). The BLAST sequence analysis tool. In The NCBI Handbook, Second Edition (National Center for Biotechnology Information (US)).
91. Jarraud, S., Lyon, G.J., Figueiredo, A.M., Lina, G., Vandenesch, F., Etienne, J., Muir, T.W., and Novick, R.P. (2000). Exfoliatin-producing strains define a fourth agr specificity group in Staphylococcus aureus. J. Bacteriol. *182*, 6517–6522. https://doi.org/10.1128/JB.182.22.6517-6522.2000.
92. Key, F.M., Khadka, V.D., R.-G., C., Blake, K.J., Deng, L., Lynn, T.C., Lee, J.C., Chiu, I.M., García-Romero, M.T., and Lieberman, T.D. (2021). On-person adaptive evolution of Staphylococcus aureus during atopic dermatitis increases disease severity. Preprint at bioRxiv. https://doi.org/10.1101/2021.03.24.436824.

STAR★METHODS

KEY RESOURCES TABLE

REAGENT or RESOURCE	SOURCE	IDENTIFIER
Antibodies		
Capsule type-specific rabbit polyclonal antisera	Tollersrud et al.[63]	N/A
Bacterial and virus strains		
S. aureus isolates	This paper	N/A
Biological samples		
Skin samples from children with atopic dermatitis	This paper	N/A
Chemicals, peptides, and recombinant proteins		
Blood agar	BBL™ Blood Agar Base (Infusion Agar)	90000-048
PCRClean-DX SPRI beads	Aline Biosciences	C-1003-250
Polyethylene glycol (PEG) 8000	Hampton Research	HR2-535
ReadyLyse Lysozyme Solution	EpiCentre	R1810M
KAPA HiFi HotStart ReadyMix	Roche	7958927001
Tryptic soy agar plates	Hardy Diagnostics	A10
Nitrocellulose BA85 filters	Whatman, Inc.	Cat#09301102
Trypsin, bovine pancreas	Fisher Scientific	Cat#AAJ6368803
Skim milk	BD BBL™/Difco™	Cat#DF0032173
Tween 20	Millipore Sigma	Cat#P1379
KPL 1-Component TMB Membrane Peroxidase Substrate	ThermoFisher Scientific	Cat#002019
Fusidic acid	Sigma-Aldrich	CAS: 6990-06-3
ChromAgar Colorex *S. aureus*	DRG international inc	Cat # TA672
Critical commercial assays		
Wizard Genomic DNA purification kit	Promega	A1120
Illumina Tagment DNA TDE1 Enzyme and Buffer Kits	Illumina	20034198
PlexWell library prep system	seqWell	plexWell 384
Puritan™ Opti- Tranz™ Liquid Amies Media Transport Tube with Rayon Tip Swab, Polysterne Handle	Puritan	LA-61PR
Puritan™ Opti- Tranz™ Liquid Amies Media Transport Tube with Miniature Rayon Tip Swab, Aluminum Handle	Puritan	LA61SAR
Experimental models: Organisms/strains		
C57BL/6 female mice	Jackson Laboratories	Strain #:000664
Deposited data		
Raw sequencing data	This paper	Genbank: PRJNA715375, PRJNA715649, PRJNA816913
Software and algorithms		
All original code	This paper	https://github.com/keyfm/aureus_ad
Python (v3.7.3)	N/A	https://www.python.org/
Snakemake (v5.4.2)	Mölder et al.[64]	https://snakemake.github.io/
MATLAB (v2015b, v2018a)	Mathworks	https://www.mathworks.com/products/matlab.html
Cutadapt (v1.18)	Martin[3]	https://cutadapt.readthedocs.io/en/stable/

(*Continued on next page*)

Continued

REAGENT or RESOURCE	SOURCE	IDENTIFIER
Sickle (v1.33)	Joshi and Fass[65]	https://github.com/najoshi/sickle
Bowtie 2 (v2.2.6)	Langmead and Salzburg[66]	http://bowtie-bio.sourceforge.net/bowtie2/index.shtml
SAMtools (v1.5) and BCFtools (v1.2)	Danecek et al.[67]	https://github.com/samtools/
Kraken 2 (v2.0.8)	Wood et al.[68]	https://github.com/DerrickWood/kraken2
BLAST (v2.7.1)	NCBI	https://blast.ncbi.nlm.nih.gov/Blast.cgi
PHYLIP (v3.69)	Felsenstein[69]	https://evolution.genetics.washington.edu/phylip.html
FigTree (v1.4.4)	N/A	https://github.com/rambaut/figtree
SPAdes (v3.13)	Bankevich et al.[70]	https://github.com/ablab/spades
Prokka (v4.8.1)	Seeman[71]	https://github.com/tseemann/prokka
CD-HIT (v4.8)	Fu et al.[72]	http://weizhong-lab.ucsd.edu/cd-hit/
treeTime	Sagulenko et al.[73]	https://github.com/neherlab/treetime
lolipop	N/A	https://github.com/cdeitrick/Lolipop
ggmueller	N/A	https://cran.r-project.org/package=ggmuller
growthrater	N/A	https://github.com/vedomics/growthrateR
SRST2	Inouye et al.[74]	https://github.com/katholt/srst2
MLST	N/A	https://github.com/tseemann/mlst
treeWAS	Collins and Didelot[58]	https://github.com/caitiecollins/treeWAS
Other		
Public *S. aureus* annotations used in annotation of assemblies	NCBI Genbank	GenBank: NC_002745, NC_003140, NC_002758, NC_002774, NC_009641, NC_003923, NC_002952, NC_002953, NC_005951, NC_002951, NC_006629, NC_007795, NC_007793, NC_007790, NC_007791, NC_007792
276 public *S. aureus* genomes analyzed	Harkins et al.,[25] Young et al.,[44] Edslev et al.,[45] and Harkins et al.[46]	See Table S10
Tegaderm (bio-occlusive film)	3M	1624W

RESOURCE AVAILABILITY

Lead contact

Further information and requests for resources and reagents should be directed to and will be fulfilled by the lead contact, Tami Lieberman (tami@mit.edu).

Materials availability

Bacterial isolates generated in this study are available from the lead contact upon reasonable request. This study did not generate new unique reagents.

Data and code availability

- Whole-genome sequence data have been deposited at SRA and are publicly available as of the date of publication. Accession numbers are listed in the key resources table. Metadata of each isolate including SRR identifier is available in Table S10.
- All original code has been deposited at github and is publicly available as of the date of publication. DOI is listed in the key resources table.
- Any additional information required to reanalyze the data reported in this work paper is available from the lead contact upon request.

EXPERIMENTAL MODEL AND SUBJECT DETAILS

Study cohort and sample collection

Patients were recruited from the Dermatology Clinic at the National Institute for Pediatrics in Mexico City under a protocol approved by the Institutional Review Boards of the NIP (042/2016) and Massachusetts Institute of Technology. Inclusion criteria for enrollment were: ages 5 to 18 years, diagnosis of AD according to modified Hanifin and Rajka criteria[75] and SCORAD $\geq$ 25 at first visit. Parental guardians and children 12 years of age or older provided written informed consent. Patients were excluded if they self-reported taking systemic antibiotics within the past month. Upon later chart review, we identified one patient (Pt. 15) did take antibiotics immediately prior to enrolment. We have included this patient as its *S.aureus* tMRCA and sweeping pattern did not differ from any other highly colonized patient. Of the 23 children included, 13 were female (Table S1).

Patients were sampled at up to five timepoints (Figure 1A), during which they received standard treatment for AD (described in more detail below). Some patients were additionally instructed to use dilute bleach baths (0.005%) twice weekly as part of a trial for the efficacy of bleach baths on AD treatment.[18] Some deviation from this schedule occurred due to patients' schedules, as well as the disruption caused by the earthquake in September 2017. Patients were counseled to avoid irritants and adequate use of fragrance-free moisturizers and/or emollients 3 times daily. Treatment with anti-inflammatory medication (either class II-VII topical corticosteroids or the calcineurin inhibitor tacrolimus 0.1%) was prescribed considering multiple factors including skin sites affected, severity of AD, and age of the patient. Patients were instructed to apply the topical corticosteroids 2x or 3x daily on affected sites until improvement was achieved. Once improved, patients were instructed to continue using the topical medication twice weekly on previously affected areas for two more weeks. At each clinical visit patients were re-evaluated and either instructed to stop the topical medication, change the type/class of medication, or to continue using the same medication twice daily or twice weekly based on the assessment. Detailed information about patient care was collected at each of the first 3 follow-up visits, but not at the 6 month follow up; patients continued treatment at their own discretion between the 4th and 5th visits. Overview of patient data, including treatment, is in Table S1.

METHOD DETAILS

Culturing and single-colony sequencing

Skin swabs were collected from seven different locations, spanning sites both affected and unaffected by AD, at each visit in Liquid Amies transport media (Figure 1A). Swabs were directly inoculated on mannitol salt and blood agar plates and cultured for 24h at 37°C. For each culture plate, up to 10 colonies suspected to be *S. aureus* by colony morphology were selected. These colonies were restreaked on ¼ of a blood agar plate and cultured for 24h at 37°C to obtain sufficient material for DNA extraction. DNA was extracted using the Wizard® Genomic DNA Purification Kit (Promega Corporation) for Gram-positive bacteria.

Dual-barcoded DNA libraries were constructed using the plexWell library prep system (SeqWell) for most samples and a modified version of the Nextera protocol for a small subset.[76] Libraries were sequenced on the Illumina NextSeq 500 using paired end 75bp reads to an average of 1.7M read pairs per isolate. Demultiplexed reads were trimmed and filtered using cutadapt v1.18[77] and sickle-trim v1.13[65] (pe -q 20 -l 50).

We note that sequenced *S. aureus* genomes from each patient is an imperfect measure of *S. aureus* absolute abundance. In some cases, with heavy growth, it was difficult to isolate 10 colonies. In addition, some sequenced colonies were determined not to be *S. aureus* from genomic data and excluded from the analysis and some cultured isolates did not yield sequenceable libraries due to a failure in DNA extraction or library prep – and thus could not be confirmed to be *S. aureus*. Regardless, we find good correlation between final colony count data and relative abundance inferred from 16S rRNA sequencing (Figure S2).

Assignment of isolates to lineages

Reads were aligned using bowtie2 v2.2.6 (-X 2000 –no-mixed –dovetail) against methicillin-resistant *Staphylococcus aureus* USA300-FPR3757 (RefSeq NC_007793). Candidate single nucleotide variants were called using samtools (v1.5), mpileup (-q30 -x -s -O -d3000), bcftools call (-c), and bcftools view (-v snps -q.75).[64,78]

To avoid issues arising from false-negative mutation calls, candidate variants found in at least one isolate were assessed for support of reference versus alternate alleles as described below. For each candidate variant, information for all reads aligning to that position (e.g. base call, quality, coverage), across all samples, were aggregated into a data structure for local filtering and analysis. Isolates were removed from analysis if they had a mean coverage of 7 reads or below across variant positions (208 isolates removed of an initial 1,735). To identify isolates with contamination that would inhibit reliable read calling, the frequency of the second highest allele at each position, in each sample, was calculated (minor allele frequency) and those isolates with a mean minor allele frequency above 0.03 across candidate sites were removed (21 isolates). We filtered candidate SNVs using a publicly available protocol (see data and code availability) similar to that previously published,[34] with the following filters. Basecalls were marked as ambiguous if the FQ score produced by samtools was above -30, the coverage per strand was below 2 reads, or the major allele frequency was below 0.85. Variant positions were filtered if 5% or more of all isolates were called as ambiguous (this removes most of the 'accessory' genome) or if the median coverage across strains was below 3 reads, or if no unmasked polymorphisms remained. These filters retained 60,973 SNVs across 1,506 isolates. A maximum-likelihood tree was built with RAxML v8.2.12[79] using the GTRCAT model, with rate heterogeneity disabled (-V). Sporadic isolates that were phylogenetically confined within the diversity of another patient were

likely mislabeled and removed (7 isolates removed, leaving a final total of 1,499 isolates). The phylogenetic tree was visualized with iTol.[80]

For each isolate the sequence type and clonal complex was inferred using the bioinformatic tools SRST2 (–truncation_score_tolerance 0.01 –max_unaligned_overlap 8 –min_edge_depth 8)[74] and MLST (https://github.com/tseemann/mlst). The *S. aureus* ST/CC database was obtained November 2022 (containing 7,898 allele combinations).[81] SRST2 isolate STs with identified mismatches (flagged with '?') agreed with the ST identified among other isolates of that lineage and were accepted. All isolates flagged by SRST2 as non-identifiable allele combinations ('*', 'NF') have been set 'NA'. Whenever the results of SRST2 and MLST disagreed the consensus ST was chosen, defined as the identified ST that was shared with the majority of other isolates assigned to that lineage. The ST typing results are reported for each isolate in Table S10. Isolates from patient 17 and minor lineage of patient 26 were manually assigned to CC30 after failing SRST2/MLST sequence type assignment, despite matched allele types for 6 out of 7 alleles that define CC30; the CC30 assignment is also supported by the phylogeny (Figure 1C); all other isolates that failed sequence typing (labeled NA) are not shown in Figure 1B (127 out of 1,499).

Lineages are defined as phylogenetically closely related *S. aureus* from the same patient which differ by less than 100 SNVs on the core genome (Figure S1). Analysis of minor lineage detection dependency on the number of isolates sampled at a given visit suggests that deeper sampling would have been unlikely to detect additional lineages from most patients (Figure S2E). A second phylogeny performed using the methicillin-sensitive *S. aureus* FDA209P (GenBank: NCTC 7447, RefSeq NZ_AP014942, NZ_AP014943) genome as a reference for alignment[82] resulted in the same lineage groupings (data not shown).

Within-patient phylogenetic reconstruction

We constructed lineage-specific assemblies in order to capture true genome-wide diversity; when combined with alignment, this approach can capture variants in the accessory genome not shared by all isolates.[4] For patients colonized by multiple lineages, we only analyzed isolates from the major lineage. Only isolates with $\geq$ 80% reads assigned to *S. aureus* on the species level (assigned using kraken2, default parameters, and standard database build Sep 24 2018)[68] were included for *de-novo* assembly, leaving 1,215 isolates. For each lineage, we concatenated up to 250,000 reads from each member isolate and assembled a reference genome with SPAdes[70] (v3.13, careful mode). All scaffolds of size 500b or larger were annotated using prokka[71] (v1.14.6), which was supplied with a list of proteins (*–proteins*) from nine publicly available *S. aureus* genomes and six accompanying plasmids (GenBank: NC_002745, NC_003140, NC_002758, NC_002774, NC_009641, NC_003923, NC_002952, NC_002953, NC_005951, NC_002951, NC_006629, NC_007795, NC_007793, NC_007790, NC_007791, NC_007792). The assemblies for each patient are summarized in Table S6.

We aligned the data of all initial 1,704 isolates from major lineages to their respective patient-specific assemblies using bowtie2[66] using the same parameters as described for *assignment of isolates to lineages* analysis. Isolates and candidate single nucleotide variants were processed with identical methods as listed in *assignment of isolates to lineages*, but with the following modifications: (1) To remove isolates with an inflated mean coverage across the assembled genomes due to high-copy number plasmids we required that at least 10% of the genome covered at 8X; (2) To detect variations within the accessory genome, the allowed maximum fraction of ambiguous isolates per site was increased from 5% to 25%; (3) To remove variants that emerged from recombination or other complex events, we identified SNVs that were less then 500b apart and covaried highly across isolates within a patient (a SNV was considered to highly covary with another SNV if its covariance was in the 90% percentile across covariances calculated with the focal SNV); these positions were removed from downstream analysis. (4) To remove cross-contaminated samples, isolates were omitted if they had minor mean allele-frequency of 9% across verified SNVs (removing 6 isolates of patient 19). Overall, these filters removed 284 isolates, leaving 1,422 isolates and 915 *de novo* on-person SNVs across 23 subjects (Table S7). Phylogenetic reconstruction was done using *dnapars* from PHYLIP v3.69.[69] Each lineage's tree was rooted using the isolate with the highest coverage from the most closely related lineage as an outgroup (based on *assignment of isolates to lineages* analysis).

Molecular clock and TMRCA

We estimated the number of *de novo* mutations per isolate using all positions variable within a patient lineage. The ancestral state of each variant is defined by the allele called in the lineage-specific outgroup (the isolate with the highest coverage from the most closely related lineage; see above). If this was not available, the major allele across the set of isolates used as an outgroup for any lineage was used. For Patient 26, we checked the predicted ancestral genotype using *treetime*[73] after noticing a significantly elevated molecular clock (using procedures below); we changed the ancestral allele of the outgroup at four basal mutation positions to match the best molecular clock fit predicted by *treetime*.[73] We normalized the number of mutations per isolate to the number of positions on the patient-specific assembled reference with a depth of at least 8X. We inferred the molecular rate using linear regression implemented in scipy v.1.3.1[83] and the 95% confidence interval using the two-sided inverse Students t-distribution. Time to the most recent common ancestor (tMRCA) was calculated for each patient data from each patient's earliest visit with at least 10 isolates, and the inferred uncertainty in the molecular clock was utilized to calculate the 95% confidence interval of the tMRCA. For each of the six highly colonized patients the tMRCA was calculated using their inferred mutation rate, while for all other patients the median molecular rate of the six highly colonized individuals was used (2.41×10^{-6} substitutions/site/year).

Signatures of on-person adaptive evolution

Each within-patient dataset was searched for genes with either of two signatures of adaptive evolution: parallel evolution at the gene level[1] and selective sweeps.[84–86] First, we identified cases when two or more mutations arose in a single gene within a patient, with a minimum mutation density of 1 mutation per 1000 bp. We calculated a p-value for enrichment of mutations in each gene using a Poisson distribution.[87] Only the *capD* gene in patient 12 had a significant p-value after Bonferroni correction for the number of genes on the genome (Table S4). Second, we searched for genomic positions at which the mutant allele frequency rose by at least 30% between visits. For each SNV, we assigned the ancestral allele as the allele found in the patient-specific outgroup, or, if that was not available, we used the allele present in the patient-specific assembly. We compared lists of genes with candidate adaptive signatures across patients using CD-HIT (v4.7, 95% identity).[72] All candidate signatures of adaptive evolution are reported in Table S4.

Creation of Muller plots

We visualized the change in frequency of mutations observed on each patient with $\geq$99 isolates using Mueller plots. Patient 04 and patient 15 yielded only two isolates at visit 4 and visit 2, respectively; these timepoints were omitted from visualization. We only drew mutations with an observed variation in frequency of $\geq$ 0.3 between timepoints. We converted mutation frequencies into genotype trajectories using *lolipop* v0.8.0 (https://github.com/cdeitrick/Lolipop); SNVs were grouped into a single genotype (color) if derived allele frequency difference was less than 8%. To make successive sweeps more visible, we used a custom-made python function to generate intermediate genotype frequencies between sampling timepoints. In brief, we created 100 time units per month, assumed mutations swept sequentially, and applied an exponential growth or decline following the function of frequency $x = Ɛ\text{^}((\ln(f_1) - \ln(f_0)) / g)$, with f_0 is the frequency at preceding visit or 0, f_1 is the frequency at the next visit and g is the number of time units (see data and code availability). The extended table was used again as the input for *lolipop*, which provided the input tables for plotting using the R package *ggmueller* v0.5.5.[88]

Mobile genetic element analysis

We identified genetic gain and/or loss events based on the depth of coverage of each isolate aligned to its patient-specific assembly for the six individuals with at least 99 isolates.[4] To avoid spurious results due to uneven coverage across samples or genomic regions, we calculated a z-score for each position by normalizing each isolate's depth of coverage at each position by sample and by position. We identified genomic regions greater than or equal to 5,000 bp long, for which each position's z-score was below a threshold of -0.5 with a median threshold below -1.0. Identified candidate regions were further filtered to have at least one isolate with a median coverage of 0 and at least one isolate with an average depth of at least 10X. These cutoffs were determined using a custom-made interactive python module for visualization of coverage across the entire candidate region across all samples (Table S5; see data and code availability).

Capsule typing

S. aureus capsule serotyping was performed as described previously.[89] Briefly, duplicate tryptic soy agar plates were spot inoculated in a grid pattern with *S. aureus* isolates and incubated overnight at 37°C. The colonies were blotted onto nitrocellulose filter membranes for 5 min at ambient temperature. Adherent colonies were fixed to the membranes by heating them at 60°C for 15 min. After two washes with 10 mM sodium phosphate buffer-0.85% sodium chloride (phosphate-buffered saline; PBS) to remove excess cells, the filters were immersed in a solution of trypsin (1 mg/ml; Sigma) for 60 min at 37°C to remove protein A from the bacterial cells. After two washes in PBS, the filters were blocked with 0.05% skim milk for 1 h and washed in PBS containing 0.05% Tween 20 (PBST). Each filter was incubated with capsule type-specific rabbit polyclonal antisera (diluted 1:4,000 in PBST) at 37°C for 1 h. After washing in PBST, horseradish peroxidase-conjugated donkey anti-rabbit immunoglobulin (diluted 1:5000) was incubated with each filter for 1 h at 37°C. After three washes, KPL 1-Component TMB Membrane Peroxidase Substrate was added to the filters. A purple color developed within 5 min and was scored visually from 0 to 4+. The reactivities of the clinical isolates were evaluated by comparison with those of control *S. aureus* strains (serotypes 5, 8, and nontypeable isolates) included on each filter. Results are presented in Table S3.

Growth rate

Overnight cultures were inoculated into fresh TSB at a 1:100 dilution. Cultures were grown at 37°C with shaking, for 24h in a Tecan plate reader (Infinite F Nano+, Tecan Trading AG, Switzerland). Absorbance at 595 nm was measured every 5 minutes. The plate containing growing cultures was sealed using its own lid. The growth rate was calculated using a regression on log-transformed data and selected for a single time interval across all strains where the r^2 of the estimated growth rate was > 0.999. Code and raw data available at: github.com/vedomics/growthrateR. Results are presented in Figure S12.

All experiments were performed with representative test isolates carrying *de novo* mutations in the *capD* gene from patients enrolled in this study. For each test isolate, a phylogenetically closely related and basal control isolate was chosen (see Table S7).

Fusidic acid susceptibility

Overnight cultures of patient isolates of *S. aureus* were diluted and plated on varying concentrations of fusidic acid (Sigma-Aldrich), ranging from 0.02ug/Ll to 2.5ug/mL. Both capsule positive and capsule negative strains were found to be susceptible at 0.05ug/mL, although the emergence of resistant mutants was common on both backgrounds.

Public *S. aureus* isolate genome analysis

We investigated publicly available data to verify if loss of CapD is associated with *S. aureus* colonizing AD skin. We obtained whole-genome sequence data from 4 different publications analyzing *S. aureus* in healthy individuals, AD patients, or individuals with other *S. aureus* infections.[25,44–46] When data from multiple isolates per patient was available, the isolate from the site of infection (if available) with the highest coverage was used. To examine gene content, we performed *de novo* assembly for each isolate using SPAdes (v3.13, –careful)[70] and annotated the assembly using Prokka (v1.14.6)[71] as described above. Isolates with assembly lengths of < 2.6M nucleotides were not considered and removed from consideration (removing 6 isolates). After this removal, we analyzed 276 isolates from 276 patients. To understand the relationship between isolates, we performed an alignment-based phylogenetic reconstruction using *S.aureus* COL (sequence version number: NC_002951.2, NC_006629.2) and the same filters as above. In addition, we included USA300-FPR3757 (RefSeq NC_007793) as a sample, by simulating raw reads for input to our cross-lineage phylogenetic analysis (cutting its genome in segments of size 150 b in steps of 1 b to simulate reads). The maximum likelihood phylogeny was built using RAxML v8.2.12 (-m GTRCAT)[79] and visualized with iTol.[80]

We inferred the ORF status for all capsule and capsule-associated genes using the annotated assemblies and BLAST+ v2.7.1.[90] Details about each query gene are available in Table S8. We compared the best BLAST match to each query gene for overlap with an annotated reading frame. We accepted an ORF as complete if the start and end of the best BLAST hit were each within 100 bp of a gene start or end of a single gene in the annotated assembly. *S. aureus* genomes colonizing humans are known to carry 1 of 2 predominant *cap* loci (type 5 or 8)[36] and 1 of 4 *agr* types[91] containing homologous versions of the same genes; for these cassettes we performed analysis only for the respective loci with the best BLAST match to a given isolate. Results are reported in Figures 4, S9, and S10 and summarized in Table S9. When only data from publications reporting both AD and controls are included, the enrichment of *capD* premature stop codons in AD vs controls remains significant (P=0.026).

We note that the relatively modest number of independent genomes used here, which were selected from a few studies to limit geographical bias, was not sufficient to identify genes associated with AD status in a hypothesis-free, whole-genome, approach because of the complication of linkage for bacterial association studies.[58] We identified presence / absence of genes among annotated genomes (using SPAdes and prokka as above) of the public *S. aureus* isolates using CD-HIT[72] (-s 0.9 -A 0.9 -g 1). We used TreeWAS,[58] a phylogeny-corrected method for GWAS built for asexual organisms, to identify genes associated with AD status, and identified no hits that meet genome-wide significance (Fisher's test). Our search for associations in capD presence was hypothesis-specific and thus does not require multiple hypothesis correction; nevertheless, based on the corrected p-values reported by TreeWAS for individual genes capD ranks 71 (Table S11; note that this list contains an unknown number of false positives).

in vivo infection models

In a previous version of this manuscript available on bioRxiv,[92] we reported a difference between *S. aureus* Newman WT and a Newman Cap5D deletion mutant in an epicutaneous infection model in mice. However, the two strains were found to have additional point mutations between them, including a nonsynonymous mutation in the sensor kinase *saeS* that confounded the reported impact of cap5D deletion on disease severity in this model. We repeated the experiments with bacterial isolates collected from patients enrolled in this study and observed no difference in skin infection nor skin colonization (Figure S13).

All experiments were performed with representative bacterial isolates carrying *de novo* mutations in the *capD* gene from patients enrolled in this study. For each test isolate, a phylogenetically closely related and basal control isolate was chosen. Sometimes the test isolate contained additional mutations compared to the most closely related basal isolate observed. *Patient 12*: Control: 048-RI3; Test: 059-AI7 (Q199* in *capD*; synonymous mutation in a hypothetical protein). *Patient 9*: Control: 061-N5; Test: 186-RI6 (N595S in *capD*; G278D ComE operon protein 3 *comEC*; intergenic mutation between two hypothetical proteins).

Bacteria were grown to a stationary phase overnight at 37°C in Tryptic Soy Broth (TSB) at 250 r.p.m. Stationary phase cultures were diluted 1:100 in fresh TSB and grown for 3.5 hours to approximate mid-log phase. Cultures were then centrifuged at 800xg for 15 minutes, and the resulting pellet washed twice in phosphate buffered saline (PBS). Cells were resuspended to a concentration of $\sim 10^{10}$ CFU/mL. Serial dilutions were plated on Tryptic Soy Agar (TSA) plates to confirm inoculum cell densities.

Eight-week old C57BL/6 female mice from Jackson Laboratories (Bar Harbor, ME, USA) were housed in specific pathogen free animal barrier facilities at MIT in individually ventilated isolator cages under a 12 h light/dark cycle with ad libitum food and water access. Euthanasia was performed by CO_2 inhalation. All animal experiments were approved by the Institutional Animal Care and Use Committee (IACUC) at MIT.

Two days prior to epicutaneous infection, mice were shaved and the remaining hair removed using depilatory cream (Nair) along the length of their back/flank. A sterile 1 cm^2 square of gauze was soaked in 100 uL of prepared *S. aureus* inoculum ($\sim 10^9$ CFU/mL for each strain, see crosshatches in figures) and applied to the flank skin. The gauze was secured using bio-occlusive film (Tegaderm, 3M) and the tape checked and repaired daily to maintain its integrity. Gauze soaked in sterile PBS was used as a control. Seven days post-inoculation, mice were euthanized by CO_2 and the dressing removed. Skin under the gauze was immediately scored for disease severity according to the following criteria: oedema (0-3), erythema (0-3), skin scale (0-3), and skin thickness (0-3) and totaled for a max skin score of "12.". A higher score indicated more severe disease/inflammation. For bacterial load, the flank skin immediately under the gauze ($\sim$1 cm^2) was excised and resuspended in 1 mL cold PBS contained in a 2 mL microcentrifuge tube. The tissue was cut into smaller pieces using sterilized scissors, two metal ball bearings (4.5 mm) were added to each tube, and the tissue was homogenized using a TissueLyser II (Qiagen, Germany) at 25 s^{-1} for 5 min. Homogenates were briefly spun down, serially diluted in PBS, and then plated for CFU counts. Bacterial identity was confirmed by plating on ChromAgar Colorex *S. aureus* (ChromAgar,

France) plates to differentiate any native microbiota that may have been present. A total of two replicates were performed. The analysis of all animal experiments was blinded. For colonization experiments, bacteria were prepared as above and $\sim 10^7$ CFU were applied to each ear in a 50 uL volume. Mice were euthanized 24 h later and tissue was harvested, homogenized, and serially diluted in PBS. Bacterial identity was confirmed by plating on ChromAgar Colorex *S. aureus* plates.

Collectors curve analysis

For each patient and sampling point (visit) with at least 10 isolates a collector curve was created for dMRCA or identified SNVs (Figures S14 and S15). For each patient-visit dataset we re-sampled with replacement $0 < x < n$ isolates each x sampled 100 times, calculated the within-sample diversity, and plotted the mean and standard deviation.

QUANTIFICATION AND STATISTICAL ANALYSIS

Information on the statistical tests and simulations can be found in the figure legends and in the corresponding method details. Statistics for all genomic analyses were computed in python and statistics for growth curve analyses were computed in R. All code is available github (see key resources table).